Functional specialization within the inferior parietal lobes across cognitive domains

Short title: Specialization in the inferior parietal cortex

Ole Numssen[1], Danilo Bzdok[2,3,†,*], Gesa Hartwigsen[1,†,*]

[1] Lise Meitner Research Group "Cognition and Plasticity", Max Planck Institute for Human Cognitive and Brain Sciences Leipzig, Germany

[2] Department of Biomedical Engineering, McConnell Brain Imaging Centre, Montreal Neurological Institute, Faculty of Medicine, McGill University, Montreal, Canada

[3] Mila - Quebec Artificial Intelligence Institute, Montreal, Canada

[†] shared senior authorship

Main text: 4539 words
Materials and Methods: 3201 words
Abstract: 150 **words**

Number of Figures: 5**; Number of Tables:** 2

*Correspondence should be addressed to:

Danilo Bzdok
McConnell Brain Imaging Centre
Department of Biomedical Engineering
Montreal Neurological Institute
3801 rue University
Bureau #872D
Montréal (Québec) H3A 2B4, Canada
Phone: +1 438 524 2713
danilo.bzdok@mcgill.ca

Gesa Hartwigsen
Lise Meitner Research Group
Cognition and Plasticity
Max Planck Institute for Human
Cognitive and Brain Sciences
Stephanstrasse 1a
D-04103 Leipzig, Germany
Phone: +49 341 9940162
hartwigsen@cbs.mpg.de

Abstract

The inferior parietal lobe (IPL) is a key neural substrate underlying diverse mental processes, from basic attention to language and social cognition, that define human interactions. Its putative domain-global role appears to tie into poorly understood differences between cognitive domains in both hemispheres. Across attentional, semantic, and social cognitive tasks, our study explored functional specialization within the IPL. The task specificity of IPL subregion activity was substantiated by distinct predictive signatures identified by multivariate pattern-learning algorithms. Moreover, the left and right IPL exerted domain-specific modulation of effective connectivity among their subregions. Task-evoked functional interactions of the anterior and posterior IPL subregions involved recruitment of distributed cortical partners. While anterior IPL subregions were engaged in strongly lateralized coupling links, both posterior subregions showed more symmetric coupling patterns across hemispheres. Our collective results shed light on how under-appreciated functional specialization in the IPL supports some of the most distinctive human mental capacities.

Keywords: human intelligence, systems neuroscience, lateralization, human cognition, language, attention, social cognition, machine learning

Introduction

Many cognitive processes are realized by spatially distributed neural networks in the human brain. The inferior parietal lobe (IPL) is a heteromodal convergence zone of various brain networks that is central to realizing key cognitive operations across different levels of the neural processing hierarchy (Kernbach et al., 2018; Seghier, 2013). These mental operations include lower-level processes, such as spatial attention, as well as higher-level processes that are distinctly elaborate in the human species, like semantic memory and modes of social exchange.

During primate evolution, the IPL has probably undergone remarkable expansion and functional reorganization (Van Essen & Dierker, 2007; Xu et al., 2020). The emergence of new areas inside the human IPL has been seriously considered (Mars et al., 2013), while its precise correspondence to nonhuman homologues is still debated (Seghier, 2013). The evolutionary trajectory of the IPL, as part of the recent cortical expansion in humans may bear important relationships to language ability, future planning, problem solving, and other complex mental operations (Seghier, 2013) at which humans excel.

Diverse cognitive capacities have been linked to neural activity in the IPL. Among these, spatial attention is crucial in an ever-changing environment that requires rapid behavioral adaptation (Corbetta et al., 2008). Systematic reviews have identified the right IPL as a key region for visuospatial attention (Corbetta et al., 2008). Accordingly, neurological damage of the right IPL entails a clinical condition called hemi-neglect: the failure to orient visual attention to the contralesional side (Morrow & Ratcliff, 1998). In contrast to visuospatial attention, language function is widely accepted to lateralize to the (dominant) left hemisphere (Friederici, 2017). Tissue damage to the left temporo-parietal cortex has been reported, for decades, to cause impairments of semantic processing – key to reading and other elaborate forms of language comprehension (Binder et al., 2009; Hartwigsen et al., 2016; Seghier, 2013). Semantic processing is instrumental for the human ability to contextualize and act according to the meaning of objects, events, and situations (Lambon Ralph & Patterson, 2008).

Moreover, semantic concepts are an integral component of numerous high-level cognitive operations, and are suspected to contribute to both social cognition and language from early development to adulthood (Binder & Desai, 2011). Semantic processing is presumably closely intertwined with social cognition. This view receives support from previous reports on spatial overlap between both cognitive domains in the left IPL (Bzdok et al., 2016; Mars et al., 2011; Seghier, 2013). However, many human neuroimaging experiments have shown that advanced social cognitive functions, such as the capacity to infer others' thoughts, beliefs, and behavioral dispositions, tend to engage the IPL in both hemispheres (Bzdok et al., 2016).

Substantiating these earlier hints at functional specialization of left versus right IPL, both regions also differ on the structural level. Architectural heterogeneity is indicated by cytoarchitectonic borders and gyral differentiation (Caspers et al., 2008) as well as anatomical fiber bundle connections as quantified by fiber tractography (Caspers et al., 2011). Such heterogeneity in the IPL is not only found between individuals, but also between the left and right hemisphere (Toga & Thompson, 2003). This structural scaffold has the potential to support the unique neurocognitive properties of the left and right IPL.

Finally, the IPL harbors a major hub of the transmodal association network (Braga et al., 2019) ('default mode network') and is densely connected with other cortical key areas for various functions. This is reflected in intimate functional interactions with several other large-scale brain networks as measured by intrinsic functional connectivity (Buckner & DiNicola, 2019). Despite indications in favor of lateralized functional specialization for human-defining cognitive domains, it remains unclear how the left and right IPL interact with distributed neural networks to realize advanced cognitive operations like social and semantic processes.

For these reasons, our study capitalized on cognitive neuroimaging experiments that tap on multiple functional domains. The combination of an arsenal of data-driven analysis techniques allowed zooming in on the functional specialization and brain-wide interaction profiles of the IPL and its segregated components. Our well-matched experimental paradigms prompted attentional

reorienting, lexical decisions, and mental perspective taking – archetypical processes that exemplify the broader cognitive domains attention, semantics, and social cognition. The direct task comparison in the same sample of subjects enabled us to identify functional specialization and involvement of common mechanisms across attentional, semantic, and social realms of human cognition. Our unique characterization of IPL function, subspecialization, and interaction patterns provides key insights into cognitive operations that underlie elaborate forms of human interaction and communication.

Results

IPL recruitment in different cognitive tasks: neural activity responses

We designed three different tasks to probe the three domains of interest. An attentional reorienting task required subjects to make spatially congruent button presses in response to visually presented cues. A lexical decision task probed visual word-pseudoword decisions and a mental perspective taking task prompted decisions on the mental beliefs of others (Fig. S1 for the experimental design and behavioral results).

We first examined neural activity responses for each task separately by contrasting each target condition (*invalid*, *word*, *false belief*) with its respective control condition (*valid*, *pseudoword*, *true belief*). In this analysis, all tasks showed increased neural activity in a widespread set of brain regions, including the IPL.

Attentional reorienting task

Relative to the control condition, we found that the attentional reorienting condition significantly modulated neural activity in several nodes of the default mode network, including the right inferior parietal lobes (IPL) (supramarginal gyrus) and to a lesser extent also the left IPL (supramarginal gyrus), as well as the bilateral precuneus. Key nodes of the dorsal attention network were also activated, including the left frontal eye field and superior parietal lobe.

Lexical decision task

Compared to pseudoword processing, real word processing predominantly activated left-hemispheric parts of the default mode network, including the IPL (angular gyrus) and middle cingulate gyrus, as well as the superior frontal gyrus.

Social cognition task

As expected, the results for the social cognition task were less strong (Rothmayr et al., 2011; Sommer et al., 2010). Uncorrected peak activations for the false belief relative to the true belief task encompassed bilateral areas, including the supplementary motor cortex, inferior frontal gyrus and precentral gyrus. To a lesser extent, nodes of the default mode network were also engaged, including the left precentral gyrus, right IPL (angular gyrus), and bilateral precuneus.

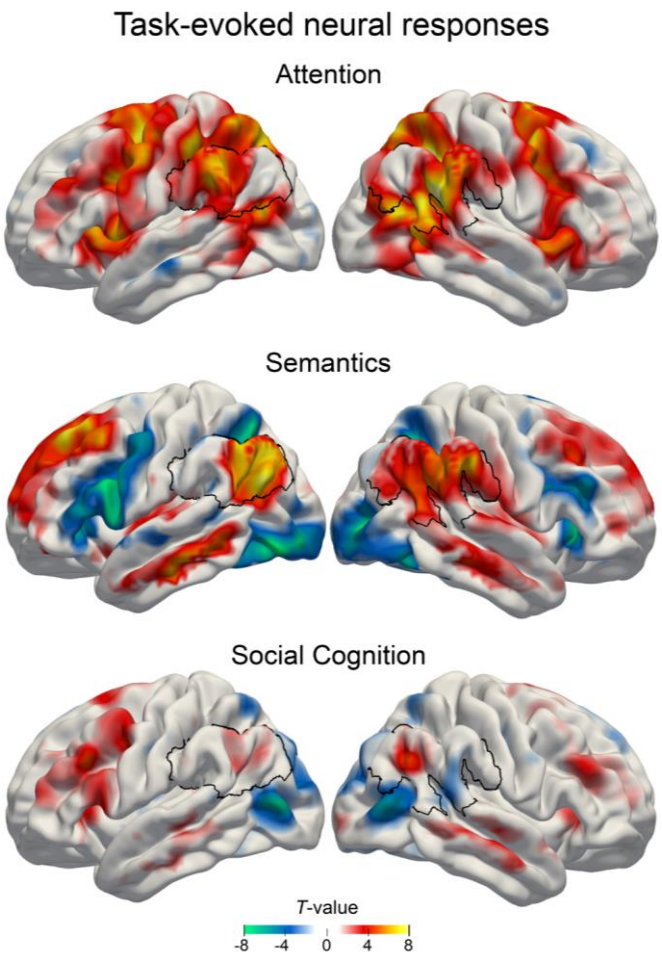

Fig. 1. Main effects of estimated neural activity in the three cognitive domains. Task-dependent BOLD responses were quantified using common mass-univariate analyses at the whole-brain level. **Attentional reorienting task.** *invalid* > *valid* contrast. **Semantic task.** *word* > *pseudoword* contrast. **Social cognition task.**

false belief > *true belief* contrast. Colors indicate unthresholded T-values for display purposes. Warm colors: higher GLM beta estimates for the target conditions. Cold colors: higher GLM beta estimates for the control condition. Black outline: region of interest in the inferior parietal lobe. Experimental design and behavioral results: Figure 1–figure supplement 1

For details on task-specific activity patterns, see Fig. 1 and Table S1.

To summarize neural activity responses in the IPL, we found strong upregulation of the right supramarginal gyrus (x, y, z = 57, -48, 24; T = 9.68) during attentional reorienting, left angular gyrus (x, y, z = -51, -72, 28; T = 8.00) during lexical decisions, and right angular gyrus (51, -60, 31; T = 5.15) during perspective taking. Standard mass-univariate analyses showed that all three tasks recruited areas within the larger IPL region in at least one hemisphere.

Functional parcellation of the IPL in two subregions

To isolate coherent structure-function mappings from neural task responses, we used data-driven clustering algorithms to separate the cytoarchitectonically constrained region of interest (ROI) in the IPL into subregions (see Methods for details). According to the applied cluster validity criteria, a two-cluster solution was indicated to be optimal in each hemisphere considering different cluster numbers. The choice of two final clusters was based on majority votes yielding 97.1% and 78.8% agreement across 25 distinct cluster validity criteria (cf. Methods) for left and right IPL, respectively (Table 1). The three-cluster solution emerged as the second best choice (left IPL: 2.8% agreement, right IPL: 21.2% agreement).

To investigate the possible influence of general motor responses within the IPL on our results, we estimated a third set of GLMs ($GLM_{cond+RT}$), which was based on the initial GLM_{cond} with one additional regressor that modeled reaction times for all three tasks. This reaction time regressor captured unspecific motor preparation and execution components that were not of interest here. The task-dependent BOLD responses closely resembled the results from the original analysis (Figure 3–figure supplements 2). The data-driven clustering based on these results selected a similar parcellation

solution with comparable certainty. 95.3% and 73.0% of the majority votes selected a two cluster solution for the left and right IPL respectively, based on $GLM_{cond+RT}$. 82 voxels in the left IPL and 73 in the right IPL were unstable across random initializations. The cluster similarity across solutions is illustrated in Figure 3–figure supplement 3.

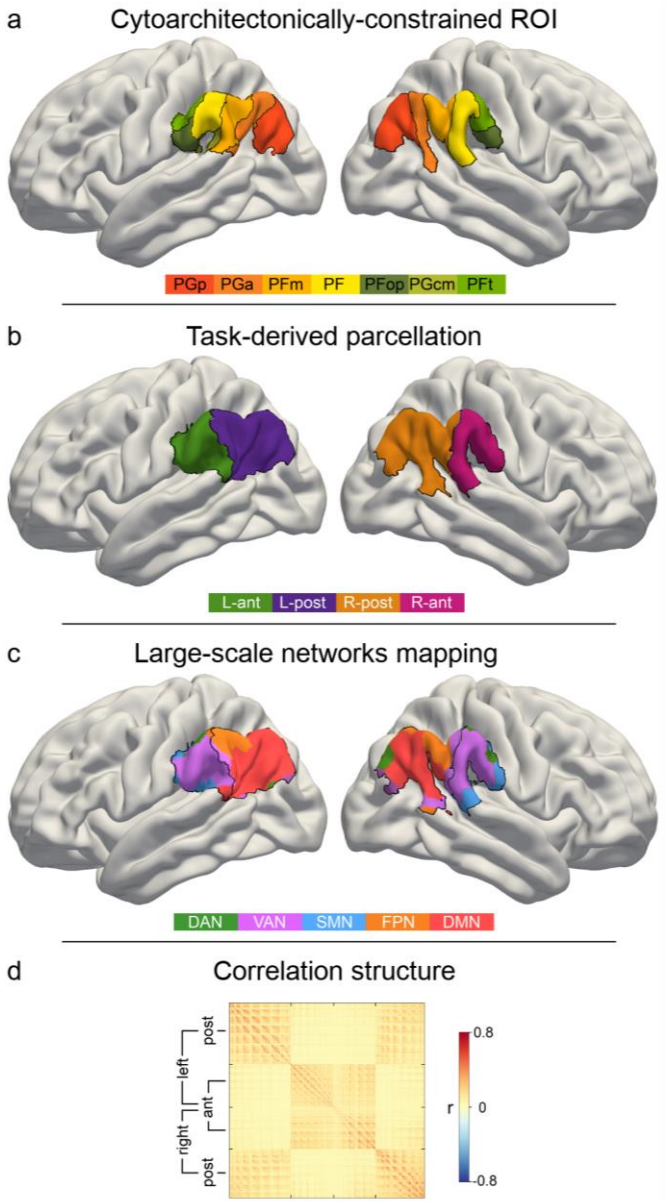

Fig. 2. IPL parcellation extracted from neural activity responses across attention, semantics, and social cognition. Neural activity estimates from all three task experiments were pooled to achieve a data-driven segregation of the inferior parietal lobe, separately in each hemisphere. **(a)** Cytoarchitectonic boundaries defined the contours of our region of interest (ROI) (Zilles & Amunts, 2010). **(b)** The derived ROI was submitted to automatic parcellation into subregions to capture neural activity profiles of the three domains in each hemisphere. L-ant: left anterior subregion. L-post: left posterior subregion. R-ant: right anterior subregion. R-post: right posterior subregion. **(c)** Mapping of large-scale brain networks (Yeo et al., 2011) to the ROI. Posterior subregions are predominantly populated by the default mode network (DMN), while the

anterior regions mainly host the ventral attention network (VAN). DAN: dorsal attention network. FPN: fronto-parietal network. SMN: somatomotor network. **(d)** Similarity matrix of voxel-wise neural activity estimates of single trials, reordered according to (c). The similarity structure reproduces the parcellation results.

Hemispheric symmetry of the final IPL parcellation: Figure 2–figure supplement 1

Task-evoked neural responses in the IPL with explicit motor preparation modelling: Figure 2–figure supplement 2

Explicitly modelling motor preparation yields a similar clustering solution: Figure 2–figure supplement 3

For all later analysis steps, 74 (out of 1102) voxels in the left and 84 (out of 1123) in the right IPL ROI were removed from the final solution because their cluster assignments were unstable across the random centroid initializations of the k-means algorithm. All discarded voxels were located at the cluster borders. The IPL parcellation procedure led to one anterior subregion (left hemisphere: L-ant, right hemisphere: R-ant) and one posterior subregion (L-post, R-post) in each hemisphere (Fig. 2B).

Hemispheric asymmetries in cluster assignment were evaluated by quantifying topographical overlap after flipping the right-left axis of the four derived IPL subregions (Fig. S3). Around two thirds of the voxels composing the IPL ROI (left: 64.98%, right: 66.31%) were spatially congruent across hemispheres. Considering these corresponding voxels contained in both left and right IPL ROI, subregion-specific across-hemisphere congruency was nearly perfect (L-ant: 88.97%; L-post: 100%; R-ant: 100%; R-post: 93.48%). The data-driven IPL parcellation into two subregions in each hemisphere served as the basis for all subsequent analyses.

Table 1. Task-derived IPL subregions

Hemisphere	Position	Label	Volume	Center of mass	Cytoarchitectonic area
Left	anterior	L-ant	11.6 cm^3	-57, -32, 30	PF, PFop, PGcm, PFt
Left	posterior	L-post	20.7 cm^3	-48, -61, 33	PGa, PGp, PFm, PF
Right	anterior	R-ant	12.9 cm^3	58, -29, 28	PF, PFop, PGcm, PFt
Right	posterior	R-post	19.8 cm^3	51, -57, 32	PGa, PGp, PFm

Note: Cytoarchitectonic assignment was performed with the SPM Anatomy Toolbox. Center of mass is given in MNI coordinates (x, y, z).

Task activity responses are predictive for different cognitive domains

Building on the obtained functional parcellation of the IPL into two core subregions that show different activation patterns for the probed cognitive domains, we investigated task-dependent specialization of IPL function using tools from machine learning. By deploying a linear predictive pattern-learning algorithm, we solved the classification problem of assigning task-membership from single experimental trials based on the subregion-level neural activity changes. We evaluated the quality of the predictive model via leave-one-subject-out cross-validation, that is, by testing the fitted model on data from a subject that was not used during model building. Our results indicate that neural activity response patterns from our IPL subregions alone carried relevant information that was granular enough to allow for successful task classification significantly above chance. The logistic predictive model was cross-validated in a one-versus-rest scheme to attempt classifying trial brain scans from hold-out subjects. This machine learning pipeline resulted in an overall out-of-sample classification accuracy of 52.11% (chance: 33.33%). Note that this cross-validation scheme leads to conservative accuracy estimates, as the classifier is tested on brain activity information from subjects it has not seen before. Therefore this approach provides a reliable estimate for the expected generalization in neuroimaging subjects scanned in the future (Bzdok & Yeo, 2017). Prediction accuracy reached 31.09% for the attentional reorienting task, 59.24% for the lexical decision task and 66.41% for the perspective taking task.

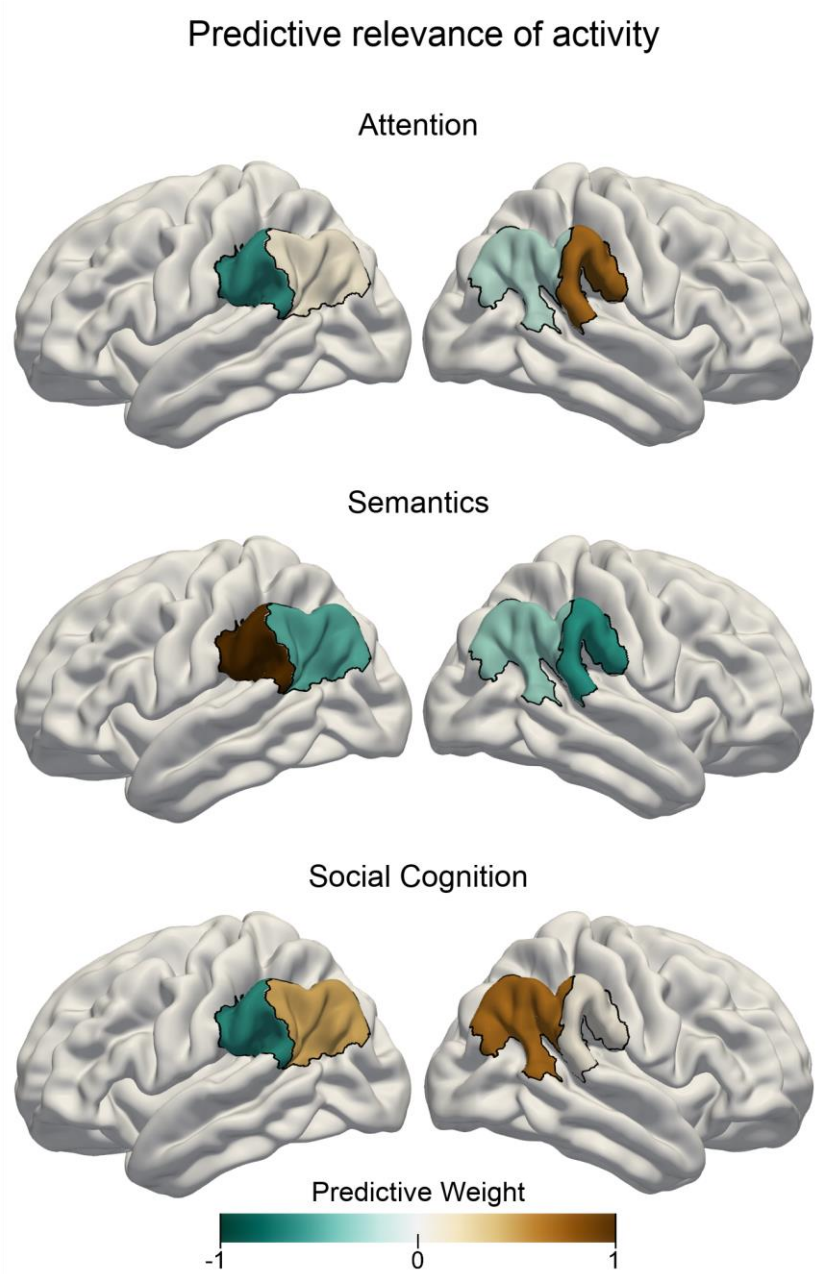

Fig. 3. Task-specific predictive contributions of IPL subregions. Pattern-learning algorithms extracted predictive rules from neural activity estimates aggregated in the left vs. right anterior vs. posterior IPL subregions from the three target experimental conditions for attentional reorienting **(top)**, lexical decisions **(center)**, and perspective taking of others' mental states **(bottom)**. Colors show the predictive signature with relative contributions of each of the four IPL subregions in detecting the presence of the three cognitive states from neural activity responses. A more positive subregion weight (brown color) for a given task implies that neural activity from this subregion carried information that increased the probability of a specific task being represented in trial brain scans. A leave-one-subject-out cross-validation was implemented to fit the predictive model. Negative values (cold colors) denote driving the prediction decision towards the respective other tasks.

Figure 3–figure supplement 1. Neural activity estimates for the target and control conditions of the three tasks.

Relative to the other two experimental tasks, increased neural activity in the right anterior subregion and less neural activity in the left anterior subregion was associated with the attentional reorienting task when considering multivariate patterns distributed across all IPL subregions (see Fig. 3). In contrast, successful trial classification pertaining to lexical decisions was driven by neural activity increases in the left anterior subregion and neural activity decreases in the right anterior subregion, relative to the other two tasks. Finally, neural activity within both posterior subregions carried salient information that was instrumental in successfully discriminating trial brain scans recorded during perspective taking.

Task-specific network connectivity resembles task complexity

We subsequently delineated the task-dependent profiles of how IPL subregions are functionally coupled with regions outside the IPL ROI. For this purpose, we assessed functional connectivity between the four IPL subregions and other cortical brain regions. By means of non-parametric permutation testing, we tested for statistically significant coupling differences (Fig. 4 and Fig. S4). The connectivity profiles between the four IPL subregions and large-scale brain networks were significantly different between tasks. The anterior subregions showed strong degrees of hemispheric lateralization and domain specificity. In contrast, the posterior subregions showed less lateralization and a higher degree of across-network coupling.

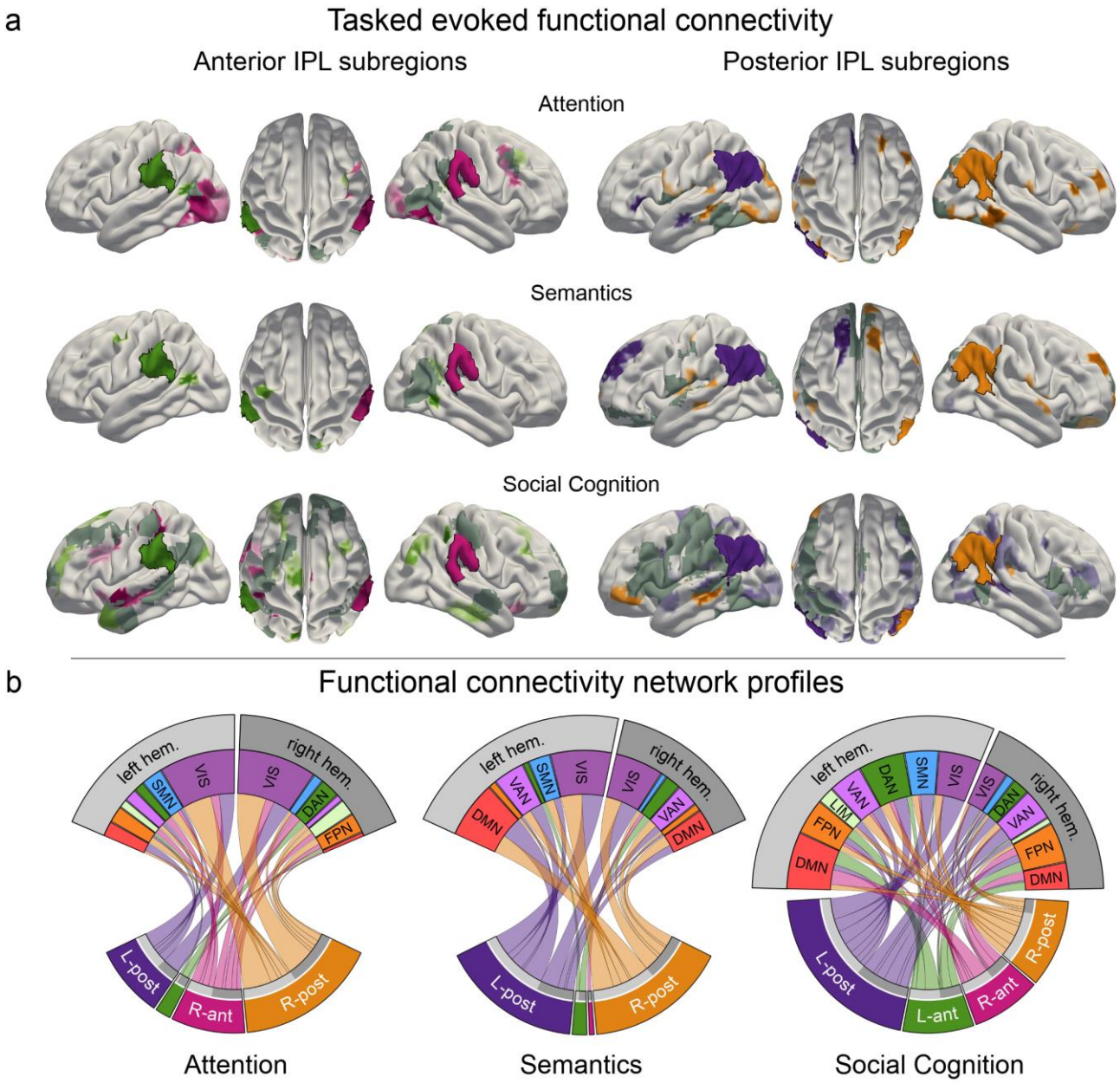

Fig. 4. Task-induced shifts in cortex-wide functional connectivity. Task-dependent functional connectivity profiles of the four IPL subregions with other coupling partners, compared to the respective other tasks. **(a)** Task-specific correlation between anterior (left) and posterior (right) IPL subregions and brain-wide cortical regions. All results are statistically significant at $p < 0.05$, tested against the null hypothesis of indistinguishable connectivity strength between a given IPL subregion and the rest of the brain across all three tasks. L-ant: left anterior IPL subregion; L-post: left posterior IPL subregion; R-ant: right anterior IPL subregion; R-post: right posterior IPL subregion. Dark gray: mutual connectivity target. **(b)** Task-specific connectivity profiles of the four IPL subregions with seven large-scale brain networks (Yeo et al., 2011). DAN: dorsal attention network. DMN: default mode network. FPN: fronto-parietal network. LIM: limbic network. VAN: ventral attention network. SMN: somatomotor network. VIS: visual network.

Subregion-specific functional connectivity: Figure 4–figure supplement 1

Task-specific connectivity profiles for anterior IPL subregions

During attentional reorienting, the right anterior IPL subregion was stronger involved in cortex-wide connectivity than its left-hemispheric counterpart (Fig. 5A, left column; Fig. 5D). The visual network and regions belonging to the dorsal attention network emerged as its preferred coupling partners (Fig. S4). The left anterior subregion was less engaged in cortical connectivity, and showed the strongest coupling with the dorsal attention network and the fronto-parietal control network. Compared to the other two functional domains, lexical decisions led to less cortex-wide connectivity, most strongly with left hemispheric dorsal attention network regions. In contrast, the perspective taking connectivity profiles for the left and right anterior subregions showed coupling with various networks. These IPL subregions revealed the strongest coupling patterns with left-hemispheric default mode network and bilateral fronto-parietal control network regions.

Task-specific connectivity profiles for posterior IPL subregions

During attentional reorienting, specific cortical connectivity shifts emerged for the right posterior subregion rather than the left posterior subregion of the IPL ROI (Fig. 5A, right column; Fig. 5D). Relative to the other two tasks, attentional reorienting led to significantly enhanced functional coupling with the visual network and left-hemispheric parts of the somatomotor network, as well as increased connectivity with right-hemispheric parts of the fronto-parietal control network (Fig. S4). Processing lexical decisions in turn was specifically characterized by coherent connectivity increases between the posterior IPL subregions and the bilateral visual network, the default mode network and the ventral attention network. Finally, engagement in perspective taking engendered significantly stronger functional connectivity for the left posterior subregion and extended parts of several large-scale brain networks. While the left posterior subregion showed similar connectivity strength to bilateral parts of large-scale networks, the right posterior subregion mainly interacted with contralateral parts. The posterior IPL regions showed connectivity links with multiple coupling partners, including regions belonging to the visual network, to the ventral and dorsal attention network, and to the somatomotor network.

Causal interactions between IPL subregions are task-dependent

To complement our findings on the task-evoked shifts in broader cortical connectivity profiles, we used dynamic causal modeling (DCM) to identify directed task-specific connectivity modulations between IPL subregions. The DCM optimization procedure provided one Bayesian parameter average group-level model. All modulatory parameters of this optimal model exceeded zero given a 95% confidence interval. Permutation-based tests provided evidence for task-specific differences in the emerging modulatory configurations among the IPL subregions (Fig. 5, see Table 2 for modulatory parameter estimates between subregions and Table S2 for other model parameters).

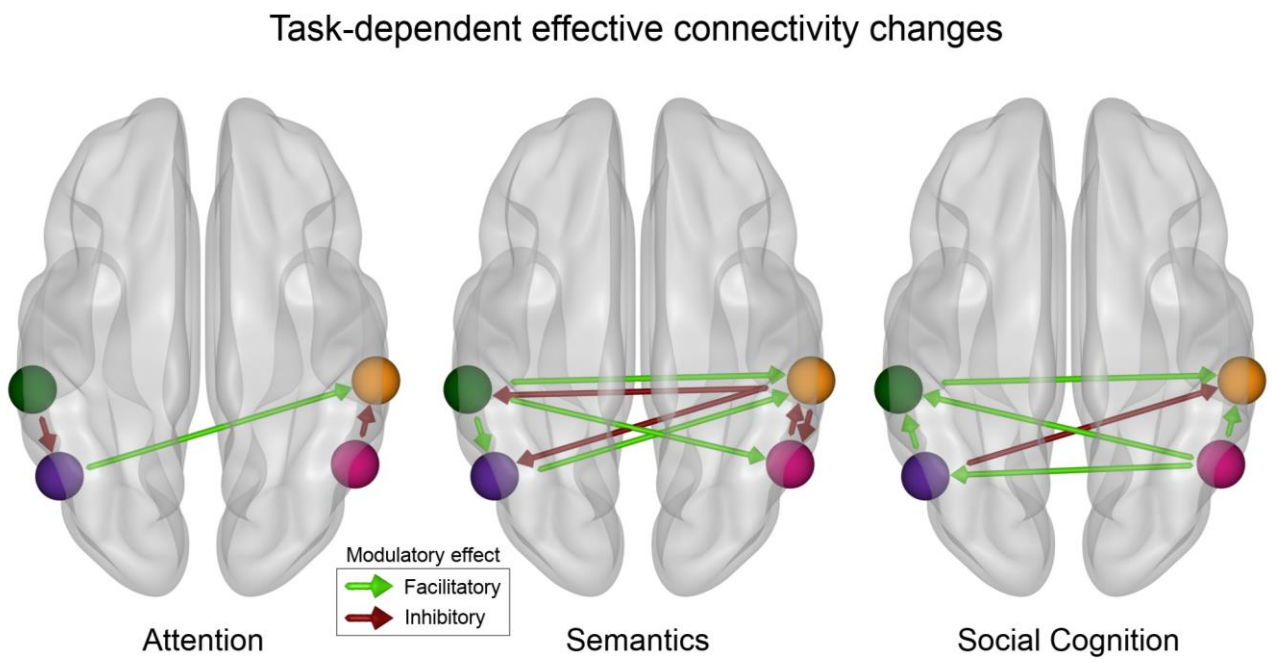

Fig. 5. Tasks cause different effective connectivity modulations among IPL subregions. The modulation assessed by dynamic causal modeling (DCM) of directed connectivity among the four IPL subregions differs between attentional reorienting, lexical decisions, and perspective taking. Only significant modulatory parameters ($\alpha \leq 0.01$) are shown (based on the non-parametric permutation analysis). Attentional reorienting induces comparatively simple connectivity modulations, while both other tasks are characterized by richer changes in the modulatory influences between subregions. Lexical decisions increase facilitatory influences from the left to the right hemisphere and inhibition from the right to the left. Perspective taking causes bilateral increases in the facilitatory influence from posterior to anterior subregions. Green: DCM node in the left anterior subregion (L-ant). Violet: DCM node in the left posterior subregion (L-post). Orange: DCM node in the right anterior subregion (R-ant). Pink: DCM node in the right posterior (R-post) subregion.

Explicitly probing modulatory effects on directed connectivity within the IPL, attentional reorienting was characterized by a simple coupling configuration, with three significant modulations: An increased inhibitory influence from the left anterior to the left posterior subregion, a facilitatory drive from the left posterior to the right anterior subregion, and an inhibitory influence from the right posterior to the right anterior subregion (Fig. 5, left). The attention coupling topology was distinctively closer to the intrinsic connectivity than effective modulation patterns underlying both other domains. Both other tasks prompted more complex patterns of coupling modulations among IPL subregions. During lexical decisions, we found strong interhemispheric modulations, both facilitatory and inhibitory, between IPL subregions. Strikingly, task-related connectivity increases from the left anterior subregion to all other subregions were facilitatory. In contrast, the right anterior subregion had an inhibitory influence on all other subregions (Fig. 5, center). Perspective taking was mainly characterized by increased facilitatory influences between IPL subregions, with the right posterior subregion exerting a facilitatory influence on all other subregions (Fig. 5, right panel). Interhemispheric interactions between subregions were also mainly facilitatory during perspective taking (Fig. 5, left).

To summarize, the three cognitive domains of interest were characterized by fundamentally different motifs of effective connectivity modulations among IPL subregions. A core observation relies on a simple directed connectivity profile for attentional reorienting and more complex directed connectivity interactions between IPL subregions for both higher-level tasks.

Table 2. Task-specific effective connectivity modulation

Source subregion		Target subregion	Modulation strength	p-value
Attention				
L-ant	→	R-post	-1.93	0.0017
L-post	→	R-ant	3.01	0.0033
R-post	→	R-ant	-1.50	0.0007
Semantic				
L-ant	→	L-post	1.08	0.0012
L-ant	→	R-ant	0.97	<0.0001

L-ant	→	R-post	1.27	0.0026
L-post	→	R-ant	1.26	<0.0001
R-ant	→	L-ant	-1.49	0.0031
R-ant	→	L-post	-2.45	0.0001
R-ant	→	R-post	-3.24	<0.0001
R-post	→	R-ant	-0.22	<0.0001
Social Cognition				
L-ant	→	R-ant	0.30	0.0078
L-post	→	L-ant	1.23	<0.0001
L-post	→	R-ant	-0.57	0.0013
R-post	→	L-ant	1.76	<0.0001
R-post	→	L-post	1.43	<0.0001
R-post	→	R-ant	2.13	<0.0001

Note: Significant modulatory parameters ('B-matrix', $\alpha \leq 0.01$) of connectivity between subregions. Based on a random effects permutation test for the null hypothesis 'no parameter difference between tasks'. The strength is given as posterior expectation from the optimum Bayesian parameter average model.

Discussion

The inferior parietal lobe is a foremost convergence zone of diverse mental capacities, several of which are potentially most developed in the human species. However, it remains open to question how some of the most basic and some of the most advanced cognitive processes converge and diverge in the IPL to realize human communication and interaction. To address this unresolved issue from different perspectives, we carried out a multi-method investigation that makes the functional specialization within the IPL apparent across attention, semantics, and social cognition tasks. By pooling insight from predictive, causal, and functional coupling analyses, we revealed a functional triple dissociation between the probed cognitive domains in the IPL at subregion-resolution. Based on neural activity estimates for the three domains, two distinctable subregions, one anterior and one posterior, were identified per IPL by a functional parcellation analysis. These subregions differed in their functional specialization across hemispheres and cognitive functions. The right anterior IPL

subregion showed the strongest predictive relevance for attentional reorienting while the left anterior IPL subregion was strongest associated with semantic processing. In contrast, both left and right posterior IPL were robustly engaged when subjects adopted the mental perspectives of others. Functional specialization within the larger IPL regions also differed with respect to whole brain connectivity profiles for the different subregions. In general, we observed increased connectivity with diverse large-scale networks with increasing cognitive complexity across tasks. Global connectivity profiles for the anterior IPL subregions showed strong hemispheric lateralization and domain specificity. Functional connectivity profiles for the left and right posterior subregions were similar within each task and showed a higher degree of across-network coupling. Complementary effective connectivity profiles between specialized IPL subregions also differed across domains, supporting the notion of stronger coupling with increasing cognitive complexity. The degree of functional specialization of the IPL has been contemplated before (Seghier, 2013). Yet, only in recent years, direct comparison of task experiments from different cognitive neuroscience domains, conventionally studied in isolation, has enjoyed increasing attention (Bzdok et al., 2013, 2016; Igelström et al., 2016). Our present study invigorates these beginning endeavors to transcend cognitive fields that are typically studied independently by separate research communities. We strive towards such cross-pollination across disparate literature streams.

To pursue this goal, we show that domain-specific functional signatures became apparent within the IPL when interrogating neural activity responses to tasks, derived predictive principles, as well as modulations of directed connectivity among IPL subregions and their functional coupling profiles with distributed brain regions. It is a key advantage that our findings were based on carefully controlled experimental paradigms that were administered to the same subject sample. Consequently, our study offers critical new elements of synthesis that pave the way for a more holistic perspective of IPL specialization.

First, the right IPL showed strong engagement in attentional processes in our study. Previous work has demonstrated a causal relation between tissue damage to the right IPL and left spatial neglect

(Thiebaut de Schotten et al., 2014). Such neurological patients routinely fail to process cues in their contralesional visual field. Additionally, transient virtual lesions of the right, but not left IPL in the intact human brain were reported to cause performance declines during attentional reorienting (Rushworth et al., 2001). Our findings corroborate and detail this previous research by carefully locating attentional processing and accompanying functional coupling shifts preferentially in the anterior subregion of the right IPL, compared to semantics and social cognition. Moreover, neural activity in the right anterior IPL subregion contained information that enabled successfully discriminating attentional reorienting from semantics and social cognition in our predictive modeling analyses. The new insights on right-hemispheric lateralization of attentional reorienting in the IPL were further refined by unique and simple effective connectivity modulations between IPL subregions. Additionally, our analyses of global functional coupling patterns revealed that the right anterior IPL subregion stands out by its connections to bilateral fronto-parietal and visual-sensory networks. Together, these findings speak to a specialized neuronal infrastructure harbored within the right anterior IPL, which is especially tuned to processing demands of attentional reorienting.

Second, our results isolate strong engagement of the anterior subregion of the left IPL for semantic processing. Deficits in various facets of semantic processes, such as in Wernicke's aphasia (Corbetta et al., 2015), have received evidence to be closely linked to left temporo-parietal damage (Corbetta et al., 2015; Dronkers et al., 2004; J. Fridriksson et al., 2016; Julius Fridriksson et al., 2010; Mirman & Graziano, 2012; Schwartz et al., 2011) among other regions of the language network. Consistently, transient virtual lesions of the left IPL in healthy subjects were reported to disrupt semantic task performance during language comprehension (Hartwigsen et al., 2017; Sliwinska et al., 2015). Our findings from mapping neural responses during experimental tasks and identifying most predictive subregions reliably situated semantic processing in the left anterior IPL subregion. In addition, our effective connectivity analyses revealed a motif of rich modulatory influences among IPL subregions during semantic processing compared to our other two tasks. Specifically, we found increased task-induced facilitatory coupling from the left to the right IPL, with the left anterior IPL

increasing its facilitatory influence on all other subregions during semantic processing. The strong facilitatory modulation exerted from the left to the right IPL was complemented by increased inhibition in the influence of the right on the left IPL and between right-hemispheric IPL subregions, potentially reflecting cognitive control processes (e.g. inhibition of alternative responses). This constellation of task-induced connectivity modulations is consistent with an interpretation of fine-grained interactions between left and right IPL subregions, rather than an exclusive role of the dominant left hemisphere in language processing (see also Binder et al., 2009; Hartwigsen, 2018; Hartwigsen et al., 2020).

Third, adding to the right and left anterior IPL's preferential involvement in attentional and semantic processing, respectively, our perspective taking task highlighted the posterior subregion of the IPL in both hemispheres as key regions for social cognition. This last piece of the functional triple dissociation in the IPL received support from our multivariate predictive algorithm approach, and was further annotated by our effective connectivity analyses. When subjects were concerned with inferring others' mental states, both posterior IPL subregions increased their facilitatory influence on the bilateral anterior IPL subregions. The overall task-specific connectivity configuration derived for our social cognition task was predominantly facilitatory, pointing towards tight intra- and interhemispheric interactions during mental perspective taking. A posterior-to-anterior transition of the neurocognitive processes subserved by the IPL has been proposed in previous research (Bzdok et al., 2016; Gordon et al., 2020). These authors identified the posterior IPL as relatively higher associative and more domain-general processing hub, compared to the anterior IPL subregions. More broadly, the observed bilateral IPL engagement in widely employed social cognition experiments carefully reconciles previous virtual lesion evidence on the functional relevance of the overall right (Krall et al., 2016) or left (Samson et al., 2004) IPL region for social cognitive functions.

Our compilation of findings provides a multi-perspective answer to the functional subspecialization of the IPL that spans lower and higher cognitive processes. Previous studies have hinted at or considered the possibility of several specialized subregions in the IPL (Bzdok et al., 2013,

2016; Kernbach et al., 2018). While some authors have advocated a monolithic functional role of the IPL, others advertised the possibility of functionally distinct neuronal populations in the IPL, which may be challenging to disentangle using conventional contrast analysis in neuroimaging. To the best of our knowledge, we are the first to conduct a within-subject study across such a diversity of cognitive domains. Thereby, we demonstrate that cognitive processing in the IPL can probably not be accounted for by a single account of functional specialization.

Based on our examination of three functional domains with different experimental tasks, two robust clusters of neural responses within the IPL were identified, each of which probably overlaps with several cytoarchitectonic areas. The observed functional differentiation along the anterior and posterior IPL region is consistent with previous work in human volunteers, which featured such functional gradients based on resting-state connectivity (Mars et al., 2011), meta-analytic connectivity modeling (Bzdok et al., 2016), and probabilistic fiber tracking (Caspers et al., 2011). More anterior portions of the IPL in the left hemisphere were reported to be more specifically associated with lower-level neural processing facets of language and social cognition. Instead, more posterior portions of the IPL were more specifically associated with advanced neural processing facets of both functional domains (Bzdok et al., 2016). This observation converges with the present constellation of findings. The relatively automatic lexical decision task in the present study was specifically associated with our left anterior IPL cluster, while the more complex perspective taking task was specifically associated with both posterior IPL subregions. Consistently, our functional connectivity analysis demonstrated relatively stronger across-network coupling with several cortical networks for our posterior IPL cluster.

A functional dissociation in the specialization of anterior and posterior IPL regions is further consistent with findings in non-human primates (Rozzi et al., 2008). Anterior parts of the monkey IPL are functionally specialized in somatosensory processes, whereas posterior parts preferentially process information based on visual input (Kravitz et al., 2011). The posterior part is thought to be particularly involved in navigation, that is, processing one's position in space (Crowe et al., 2004,

2005). This region is further associated with processing visual information in an external, object-centered manner (Crowe et al., 2008) compared to an egocentric processing system which is used to control body movements (Chafee et al., 2007; Snyder et al., 1998). These findings argue for increased processing complexity from anterior to posterior regions in the macaque IPL. It is however important to bear in mind that the monkey-human homologue of IPL anatomy remains insufficiently understood (Mars et al., 2013; Seghier, 2013).

A high degree of abstraction from sensory information in the macaque IPL is further substantiated by the existence of intention- and goal-specific neurons rather than pure movement-coding neurons in the macaque IPL (Fogassi et al., 2005; Rozzi et al., 2008). Notably, the IPL expanded in the primate lineage (Orban et al., 2004), while the existence of a homologue in non-human primate remains uncertain (Mars et al., 2011; Seghier, 2013). The expansion of the IPL may relate to cognitive capacities which are unique to humans, including the ability for speech and language processing as well as complex problem solving. We confirm and detail the previously reported gradient in the complexity of processing in the human IPL, which likely reflects fine-tuned functional differentiation for higher cognitive operations in humans.

Distinct functional specialization for human-defining cognitive operations in the IPL may explain differences in the connectivity profiles of the larger IPL regions between humans and macaques (e.g. Margulies et al., 2016; Oligschläger et al., 2018; Xu et al., 2020). Uncertain homologies between humans and non-human primates are accompanied by complex structure-function relationships in the human IPL. As an overarching tendency, functional organization reproduces structural organization in unimodal areas in the human brain. In contrast, functional organization is significantly less determined by structure in heteromodal brain regions (Vázquez-Rodríguez et al., 2019). Such laxer coupling of structure-function relations is observed in heteromodal association areas, including the IPL (Margulies et al., 2016). In general, functional specialization for higher cognitive operations may gradually decouple from the underlying structure (Vázquez-

Rodríguez et al., 2019). This notion is in line with the present results from our functional parcellation which does not simply follow cytoarchitectonic boundaries.

Our complementary set of findings indicate that task-specific effective connectivity modulations within and from different IPL subregions uniquely characterize each of the probed cognitive domains. For relatively low-level cognitive processes, here exemplified by attentional reorienting, task-specific coupling adjustment implicated a reduced set of coupling partners. In contrast, for more complex tasks, as exemplified by lexical decision and perspective taking, we found evidence for more elaborate coupling motifs, including dense intra- and inter-hemispheric facilitation and inhibition. Notably, there is a scarcity of existing studies directly devoted to investigating the left and right IPL in several different psychological tasks. The few existing studies committed to the effective connectivity of the IPL mainly focused on task-related connectivity changes between an IPL subregion and other areas of a specialized network for a single cognitive domain, typically in one hemisphere only (Fukuda et al., 2019; Hartwigsen et al., 2017). As such, our results usher towards a broader perspective. We complement the identification of intra- and inter-hemispheric IPL coupling patterns with strong domain-specific coupling profiles from IPL subregions to disparate cortical partners from large-scale brain networks.

Task-induced shifts in functional connectivity revealed key distinctions in interactions with major brain networks. Functional coupling profiles varied significantly between the three experimental tasks. Across domains, coupling partners were recruited from various large-scale brain networks. Our observation reinforces the notion of the IPL interfacing multiple neural systems and different levels of neurocognitive abstraction (Bzdok et al., 2013; Seghier, 2013).

Moreover, we show that the task-specific coupling profiles between IPL subregions and a variety of cortical partners are anchored in the functional compartments uncovered in the IPL. The wider functional connectivity profiles for the anterior and posterior subregions further elucidate their features of underlying neural processing. As a tendency, functional connectivity profiles for the left and right posterior subregions were similar within each task. Yet, global connectivity profiles varied

between the left and right anterior subregions of the IPL. The hemisphere-specific functional coupling for the anterior IPL subregions is broadly consistent with the common reports of right-hemispheric specialization of attentional reorienting processes (Rushworth et al., 2001; Schuwerk et al., 2017) and left-hemispheric specialization for semantic processes (Binder et al., 2009; Braga et al., 2019; Hartwigsen et al., 2016). The rich connectivity profiles of the left and right posterior IPL subregions support the notion of bilateral IPL relevance for social cognitive processes, consolidating previous findings (Bzdok et al., 2013, 2016).

Specifically, during attentional processing, the dedicated coupling partners of the right anterior IPL subregion included regions of the visual cortex and the dorsal attention network. During semantic processing, the left anterior subregion enhanced coupling with regions of the default mode and ventral attention network. Ultimately, during social cognition processing, the left and right posterior IPL subregions preferably coupled with the default mode network. The observed task-specific functional coupling of the posterior subregions with major brain networks was largely symmetric across both hemispheres.

To summarize our integrated experimental and computational study, we provide evidence for a functional triple dissociation in the human IPL, with task-specific functional specialization in distinct IPL subregions. This emerging view is supported by information carried in precise multivariate predictive signatures. Zooming into task-specific coupling motifs among IPL subregions, our effective connectivity analyses revealed that attentional reorienting mediated simpler coupling modulations, while semantic and social cognition were realized by more complex inter-hemispheric influences. Delineating task-evoked shifts in functional coupling patterns, in turn, uncovered that the posterior IPL subregions were linked to bilateral, symmetric recruitment of distributed cortical coupling partners, reminiscent of the default mode network. Conversely, the anterior IPL subregions were engaged in flexible and hemisphere-specific coupling patterns with brain-wide cortical partners. Together, our results shed new light on how currently under-appreciated activity and connectivity profiles within the left and right IPL support some of the most distinctive mental capacities in humans.

Materials and Methods

Subject sample

Twenty-two healthy, native German speakers (11 female, mean age 27.9 ±3.28 years) participated in this neuroimaging investigation. All subjects had normal or corrected-to-normal vision and no contraindications against magnetic resonance imaging (MRI). Subjects were recruited from the inhouse database at the Max Planck Institute for Human Cognitive and Brain Sciences. Written informed consent was obtained from all subjects before the experiment. All subjects were right-handed (laterality index ≥80% (Oldfield, 1971)). The study was performed according to the guidelines of the Declaration of Helsinki and approved by the Ethics Committee of the Medical Faculty of the University of Leipzig, Germany.

Experimental design

The functional MRI (fMRI) investigation (see Fig. S1A) consisted of three sessions that were performed on separate days, scheduled at least seven days apart from each other. Each fMRI session was divided into four runs. In all runs, each of the three tasks (i.e., attentional reorienting, lexical decisions, and perspective taking, see below for details) was administered consecutively in a task block. Within task blocks, trials were presented in an event-related fashion. Each run consisted of 40 attentional reorienting trials (8 *invalid*, 30 *valid*, 2 *catch* trials), 40 lexical decision trials (20 *word* and 20 *pseudoword* trials), and 6 perspective taking trials (3 *false belief* and 3 *true belief* trials). Each stimulus for the lexical decision and social cognition task was only shown once per subject, while the attentional reorienting task relied on simple geometric cues that were presented repeatedly. At the beginning of each task block, instructions were presented. Task order was pseudo-randomized. Trial order and timing were defined by a genetic algorithm for optimizing detection power, using an adapted version of Neurodesign v0.2.1 (Durnez et al., 2018). All experimental tasks were administered with Presentation Software (v20.1; Neurobehavioral Systems, Berkeley, CA). Prior to the first fMRI session, subjects underwent training for all three tasks outside the MRI scanner.

Training stimuli for the semantic and the social cognition task were not included in the main experiment.

Tasks

For each probed cognitive domain, we elected a well-established task. Task presentation and response selection were carefully matched across tasks, including visual stimuli and binary choices for all tasks. All three tasks conformed to the principle of using a single target condition and a single control condition to isolate the neural activity of the particular cognitive function. In all three tasks the subjects responded to a binary choice after each trial via single button press on a two-finger response box with their right hand. Button assignments for the semantic and social cognition tasks were initially pseudo-randomized across subjects, and kept identical across sessions per subject. The button box was fixated on the subject's right thigh to assure a comfortable, natural, and stable lying position in the MR scanner. Subjects were instructed to respond as fast and accurately as possible. Example trials for each of the different tasks and conditions are available in Fig. S1.

Attention

We used a Posner-like attentional reorienting task, as described previously (Rushworth et al., 2001). Each trial started with the presentation of two rectangular, empty boxes (size 2.6° of visual angle, center distance 8.3°, positioned horizontally) and a fixation cross at the center of the screen (Fig. S1B). After an average duration of 3.2 s (SD = 1.41 s, minimum interstimulus interval = 2 s), the fixation cross was replaced with an arrow pointing either to the right or the left for 250 ms or 350 ms (the 'cue'). Subsequently, a target asterisk was presented in one of the rectangles. In 75% of the trials, the target location was congruent with the direction of the arrow (*valid* condition). In 20% of the trials, the target was presented on the (unexpected) opposite side (*invalid* condition). In 5% of the trials, no asterisk was shown (*catch* condition) and no response was probed to ensure constant attention. Subjects were asked to indicate the location of the target with a button press. Note that the *invalid* condition was intended to recruit attentional reorienting processes. Instead, the *valid* condition served as the matched control condition.

Semantics

We administered a lexical decision task that contrasts words and pseudowords as a prototypical example of semantic processing (Binder et al., 2003). 240 concrete German nouns were selected from the SUBTLEX-DE database (Brysbaert et al., 2011). Inclusion criteria were i) two syllables; ii) frequency per million > 1; iii) concreteness ratings < 4; and iv) arousal ratings < 6, according to the LANG rating (note that smaller values correspond to a higher concreteness (Kanske & Kotz, 2011)). All word stimuli denoted countable entities and were non-ambiguous. A pseudoword was created for each word with Wuggy v0.2.2b2 (Keuleers & Brysbaert, 2010) to assure phonotactic validity without semantic content. Pseudowords matched their word counterparts in length, syllable structure, and transition frequencies between subsyllabic elements. Each trial started with the presentation of a fixation cross for at least 2 s (M = 3.8 s, SD = 1.7). Thereafter, a *word* (target condition) or *pseudoword* (control condition) was shown for 1 s. Subjects were instructed to indicate whether the stimulus represented a word or pseudoword via button press (Fig. S1C).

Social cognition

For the perspective taking task, we employed an adapted version of the Sally-Anne paradigm, which is known to prompt reasoning about the mental state of others (Rothmayr et al., 2011). In total, 72 three-picture comics were presented, with 2 s presentation time per stimulus. Between trials, a fixation cross was shown for at least 2 s (M = 3.8 s, SD = 1.7 s). In all trials, character A puts an object into a container-like object (picture 1). Then character B passes the object on to another container. Character A either observes this action (*true belief*) or not (*false belief*) (picture 2) and then searches in either the correct or in the wrong location (picture 3). Subjects were instructed to indicate whether the search location was congruent or incongruent with character A's knowledge about the object position via button press (Fig. S1D). A correct response during a *false belief* trial (target condition) required the subject to infer the mental state of character A from the comic narrative. In contrast, for the control condition (*true belief*) a correct response did not depend on perspective taking and could be accomplished by relying on the physical reality shown to the subjects.

Functional magnetic resonance imaging

fMRI data acquisition was performed on a 3 Tesla Siemens Prisma system (Siemens, Erlangen, Germany). A whole brain gradient echo planar (GE-EPI) T2* sensitive sequence (3x3x3.2 mm, 0.32 mm gap, TR 0.5 s, 36 slices, TE 24 ms, flip angle 45°) with multiband acceleration was used (Feinberg et al., 2010). Additionally, a high-resolution (1x1x1 mm voxel size) structural MR image (T1w) was acquired for each subject using a standard three-dimensional MPRAGE sequence.

Preprocessing

The raw fMRI data was despiked with 3dDespike from the AFNI toolbox through Nipype v1.5.0 (Gorgolewski et al., 2011). Subsequently, the preprocessing was implemented in fMRIPrep v1.4.1 (Esteban et al., 2019), a Nipype based tool. The individual T1 image was intensity corrected using N4BiasFieldCorrection v2.1.0 (Tustison et al., 2010) and skull-stripped using antsBrainExtraction.sh v2.1.0 with the OASIS (Marcus et al., 2007) template. Brain surfaces were reconstructed using recon-all from FreeSurfer v6.0.1 (Dale et al., 1999). A brain mask was refined to reconcile ANTs-derived and FreeSurfer-derived segmentations of the cortical gray matter in Mindboggle (Klein et al., 2017). Spatial normalization to the ICBM 152 nonlinear asymmetrical template version 2009c (Fonov et al., 2009) was performed through nonlinear registration with the antsRegistration tool 2.1.0 (Avants et al., 2008). Brain tissue segmentation of cerebrospinal fluid, white matter and gray matter was performed on the brain-extracted T1 with the fast tool (FSL v5.0.9 (Zhang et al., 2001)).

Functional data was slice-time corrected with 3dTshift from AFNI v16.2.07 (Cox, 1996) and motion corrected using mcflirt (FSL v5.0.9 (Jenkinson et al., 2002)). Distortion correction was performed with the TOPUP technique (Andersson et al., 2003) using 3dQwarp from the AFNI toolbox. This was followed by co-registration to the T1 using boundary-based registration (bbregister from FSL v6.0.1 (Greve & Fischl, 2009)) with nine degrees of freedom. Motion correction transformations, field distortion correcting warp, functional-to-anatomical transformation and T1-to-

MNI warp were concatenated and applied in a single step using antsApplyTransforms (ANTs v2.1.0) with Lanczos interpolation.

To account for motion induced artefacts, physiological noise regressors were extracted with the anatomical version of CompCor (Behzadi et al., 2007) (aCompCor). Six components were calculated within the intersection of the subcortical mask and the union of corticospinal fluid and white matter masks. Frame-wise displacement (Power et al., 2014) was calculated using the implementation of Nipype.

Statistical Parametric Mapping 12 (SPM 12, Wellcome Department of Imaging Neuroscience, London, UK) was used to spatially smooth the functional data with an 8 mm full-width half-maximum Gaussian kernel.

Specification of the general linear models

At the single-subject level, two design matrices were specified and general linear models (GLMs) were computed using SPM 12 (Wellcome Department of Imaging Neuroscience, London, UK) to estimate task-related neural activity. GLM_{cond} was designed with one regressor per condition in accordance with the standard mass-univariate analysis. The second set of GLMs (GLM_{trial}) was purpose-designed for multivariate and task-related functional connectivity analyses with one regressor per trial to gain access to trial-wise neural activity estimates (Abdulrahman & Henson, 2016). For GLM_{cond}, seven trial regressors were defined (*valid*, *invalid*, *catch*, *word*, *pseudoword*, *false belief*, *true belief*, duration 0 s). Additionally, three rest regressors for task-wise rest periods were included (duration 16 s each). Incorrect responses were modelled separately per task. One regressor per session was added to account for between session variability. To remove high-motion timepoints, one volume masking regressor was added for each volume with a frame-wise displacement value above 0.9 (Power et al., 2012), yielding an average of 10.04 masked volumes per subject. Six motion and six aCompCor (Behzadi et al., 2007) regressors were included to account for motion-induced artefacts. The design matrix for GLM_{trial} followed a similar general logic, but

included one regressor per trial, leading to trial wise-beta estimates instead of condition-wise beta estimates. Run, motion, and aCompCor regressors were added as above. GLM_{cond} was estimated on smoothed, GLM_{trial} on unsmoothed data. A high-pass filter of 128 s was applied and serial correlations were accounted for with the FAST method (Corbin et al., 2018). Global normalization was not performed and the canonical hemodynamic response function was used without derivatives.

Classical statistical analysis

For each task, two contrasts were defined at the single-subject level, including the condition of interest > $rest_{task}$ (*invalid* > $rest_{att}$, *word* > $rest_{sem}$, & *false belief* > $rest_{soc}$) and control condition > $rest_{task}$ (*valid* > $rest_{att}$, *pseudoword* > $rest_{sem}$, *true belief* > $rest_{soc}$). Task-wise contrasts (*invalid* > *valid*, *word* > *pseudoword*, *false belief* > *true belief*) were computed at the group level.

Brain results were rendered by means of Paraview v5.7.0 (Ahrens et al., 2005), circlelize v0.4.8 (Gu et al., 2014), and BrainNet Viewer v1.7 (Xia et al., 2013). To this end, results were transformed from MNI space (ICBM 152 linear (Mazziotta et al., 2001)) to the surface-based FreeSurfer fsaverage (Fischl et al., 1999) coordinate system via the nonlinear mapping Registration Fusion approach v0.6.5 (Wu et al., 2018).

Subregion identification in the IPL

The topographical outline for the left and right IPL ROI was guided by an established and freely available histological atlas. Seven cytoarchitectonic maps cover the human IPL in each hemisphere according to the widely used JuBrain probabilistic cytoarchitectonic atlas (Amunts & Zilles, 2001). These anatomical definitions of microstructurally defined areas known to exist in the IPL comprised one rostral (PGp) and one caudal (PGa) region in the angular gyrus, and five regions of the supramarginal gyrus (PFm, PF, PFop, PGcm, PFt), as provided by the SPM 12 Anatomy Toolbox v2.2b (Eickhoff et al., 2005). The outer boundary of the conglomerate of these cytoarchitectonic areas was taken as contours of our ROI in the IPL, separately in the left and right hemisphere. Both of our

ensuing ROI definitions occupied similar cortical volume: 1102 voxels in the left and 1123 voxels in the right (Fig. 2A) hemisphere.

We used tools from machine learning to explore coherent solutions to IPL segregation in the context of our experimental tasks. A k-means clustering (Hartigan & Wong, 1979) was applied at the voxel level with 1,000 random centroid initializations (Thirion et al., 2014) based on the estimates from the "target condition > rest" contrast of the GLM_{cond} in the IPL ROIs. The unsupervised clustering algorithm was applied on pooled information across subjects and separately for each hemisphere. To explore an optimal number of clusters, hemisphere by hemisphere, our choice was anchored in the majority vote taken across 25 distinct cluster validity metrics that were computed for candidate solutions with 2 to 7 clusters using NBClust v3.0 (Charrad et al., 2014). Each cluster quality metric provided a ranking of candidate cluster numbers based on a different notion of goodness-of-fit of the candidate solutions. The majority vote of these different ranking criteria provided a principled, data-driven rationale for the final cluster number that we endorsed in our study, in each hemisphere. To ensure robust voxel-to-cluster assignments, all solutions from the 1,000 algorithms initializations that resulted in the winning cluster number were merged into one final solution. Specifically, the final assignments of voxel-to-cluster responsibilities were based on agreement across the random algorithm initializations. Voxels with varying cluster allocations across the initializations were excluded from the final cluster solution (cf. Results section).

Task-predictive information of the IPL subregions

After establishing functionally defined subregions in our IPL ROIs, we directed attention to the information content available at subregion granularity. For this purpose, we carried out a one-versus-rest scheme in combination with a sigmoid-loss (logistic) linear predictive algorithm to automatically detect the task membership of single experimental trials directly from subregion-wise averaged neural activity signals. Model parameter estimation and model evaluation of predictive success were performed conjointly for the three target conditions (*invalid*, *word*, *false belief*). This modeling strategy naturally yielded a set of predictive weights for all subregions for each task. Appropriately

balanced numbers of trials were ensured for all conditions by sub-sampling to the minimum number of trials per subject and fMRI run. We exclusively considered task trials and brain scans with correct responses. Signal deconfounding removed variation that could be explained by session number, session time, subject identify or run time. A run-wise variable standardization was applied, before model estimation, by de-meaning to zero and unit-variance scaling to one. The generalization performance of the prediction accuracy was estimated via leave-one-subject-out cross-validation. In total, 22 model instances were built from the brain data so that each subject's data were held out once from the training process ('training') and exclusively used to assess the model's generalization properties ('testing'). The parameters of the predictive algorithm were averaged across all cross-validation folds to guard against noise and obtain a single aggregate predictive model solution for inspection and visualization (Kernbach et al., 2018). The parameters of the predictive algorithm were averaged across all cross-validation folds to guard against noise and obtain a single final predictive model solution for inspection and visualization (Kernbach et al., 2018). The pattern-classification pipelines were realized in the Python data science ecosystem, using especially nilearn v0.6.2 (Abraham et al., 2014) and scikit-learn v0.21.2 (Pedregosa et al., 2011). Overall, the set of multivariate predictive analyses thus aimed at revealing task-distinctive information available at subregion-level signals in our IPL ROIs.

Task-evoked functional connectivity shifts

We then quantitatively characterized the task-induced changes in distributed functional coupling profiles as anchored in each of the IPL subregions. Analogous to the multivariate pattern recognition approach (cf. last paragraph), this cortex-wide analysis was performed across the three distinct task contexts. We drew on the commonly used Schaefer-Yeo atlas v0.15.3 (Schaefer et al., 2018) with 400 parcels to parse the distributed neural activity estimates (GLM_{trial}) of the three target conditions (*invalid*, *word*, *false belief*). Consistent with the other analysis approaches, we discarded any trials with incorrect subject responses. Neural activity estimates were summarized by averaging across all voxels belonging to a given IPL subregion. For each experimental target condition, Pearson's

correlation coefficients were computed between a given IPL subregion and each of the Schaefer-Yeo parcels. To rigorously assess whether connectivity links between a specific IPL subregion and cortical parcel were reliably weaker or stronger in one task relative to the other two, a pooled permutation-based baseline was computed across all three task conditions. Task-specific functional coupling shifts were determined by statistical significance testing based on a non-parametric permutation procedure using an empirical null-hypothesis distribution (Bzdok & Yeo, 2017). The data-derived null model reflected the constellation of neural activity coupling strengths between a given subregion and other cortical regions that would be expected if task A induced similar patterns of brain connectivity, compared to the respective other tasks B and C. Following this fully data-driven analysis tactic, for each of the three tasks, the analysis directly provided brain maps of task-dependent functional connectivity profiles for the IPL subregions.

Task-specific effective connectivity modulation

After delineating (undirected) functional connectivity of IPL subregions with brain-wide cortical regions, we explicitly examined task-dependent causal interactions within the IPL. To achieve this goal, we analyzed the effective connectivity among the four IPL subregions by means of DCM. Since this approach centered on the directed interaction among the IPL subregions themselves, this analysis selectively included these four compartments. Effective connectivity was estimated with DCM 12.5 (Friston et al., 2013) implemented in SPM 12. We defined and deployed subject-wise DCMs with one target node per subregion. Subject-specific node centers per subregion were based on the peak activity across all three tasks. We ensured similar contribution of all tasks by task-wise normalization of neural activity estimates to define the subject-wise DCM nodes. The first eigenvariate from the timeseries of voxels in an 8mm sphere around this target was extracted (Zeidman et al., 2019). We exclusively included data from voxels within the upper quartile of estimated neural activity to ensure functional relevance (Seghier & Friston, 2013) and assured that all voxels fell into the respective IPL subregion. A fully connected DCM (full model) estimated all possible connections among the four IPL subregions (including self-connections) and directions of modulatory influences. The trial onsets

of the three target conditions were modeled as direct inputs to the nodes and as modulatory inputs to the inter-regional connections. Neural activity stemming from incorrect trials and control conditions was regressed out (Zeidman et al., 2019).

After model estimation, subject-wise full models were optimized for the intrinsic connections (A matrix) and modulatory inputs (B matrix) at the group level using the Bayesian model selection procedure (Friston & Penny, 2011). We decided against optimization of the input parameters (C matrix), as we selectively modeled nodes in high-order association cortex. As such, there was no obvious scientific hypothesis regarding the input to the system. The optimized, reduced model represented fixed-effects at the group level (Rosa et al., 2012). As a second-level random-effects analysis, we conducted a non-parametric permutation test on subject-wise parameters of the optimal reduced model. This layer of analysis identified those model parameters that varied significantly between tasks. Specifically, for each task, the parameter differences of the remaining two tasks were randomly shuffled 10,000 times to obtain and test against an empirical distribution for the null hypothesis (i.e., no differences between task-dependent effective connectivity). Statistical significance was determined based on the absolute parameter difference higher than 99.9% of the baseline difference, corresponding to $\alpha \leq 0.01$.

Acknowledgements

Funding: This work was supported by the German Research Foundation (BZ2/4-1, BZ2/3-1, and BZ2/2-1 to DB and HA6314/3-1 and HA6314/4-1 to GH), the NVIDIA Corporation (donation of a Titan Xp graphics card to GH), and National Institutes of Health (NIH grant R01AG068563A to DB). DB was further supported by the Healthy Brains Healthy Lives initiative (Canada First Research Excellence fund), by the CIFAR Artificial Intelligence Chairs program (Canada Institute for Advanced Research), and by Google (Research Award). GH was further supported by the Lise-Meitner excellence program of the Max Planck Society. **Competing Interests:** The authors declare that no competing interests exist. **Data Availability:** Data is made available from the authors upon reasonable request. Restrictions might apply due to the General Data Protection Regulation (EU). **Code Availability:** All self-written code that was used to prepare the experiment and for analyzing the data is made available: http:// gitlab.gwdg.de/IPLplasticity/FuncSeg

Supplementary Material

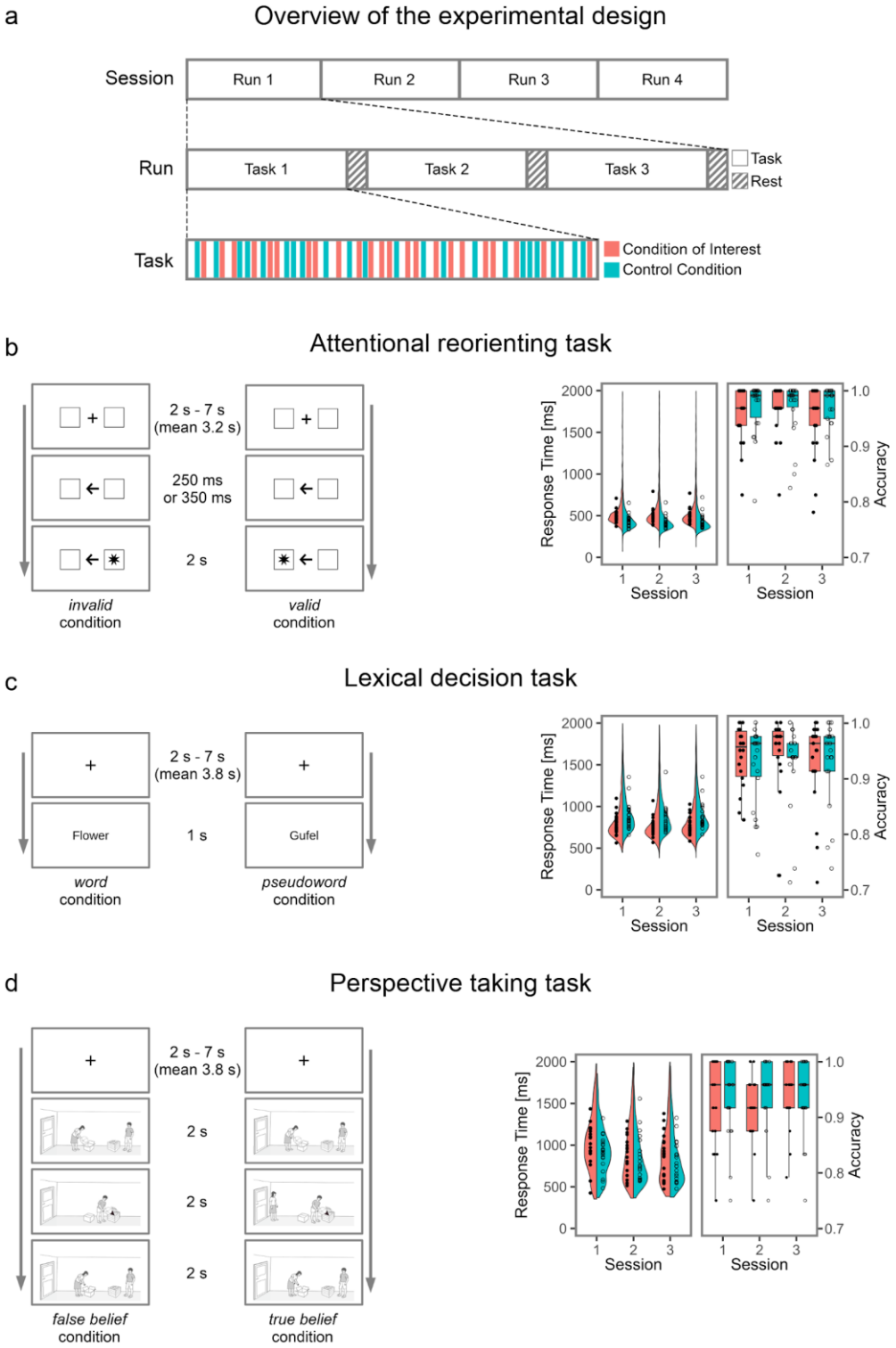

Figure 1–figure supplement 1. Experimental design and behavioral results. (a) Experimental design. Each of the four sessions consisted of four fMRI runs. In each run, all three tasks were presented in a pseudo-randomized order and analyzed in an event-related fashion. **(b) Attentional reorienting task.** In each trial, a directional arrow appeared at the center of the screen to direct the subject's attention to the left or right. In 75 % of the trials, the arrow correctly predicted the position of the target (*valid* condition), in 20 % of the trials,

the target appeared on the opposite side and subjects had to reorient their attention (*invalid* condition). In 5% of the trials, no response was prompted (*catch* condition). Subjects indicated the side of the target via button press. (**c) Lexical decision task**. Participants performed lexical decisions (*word* or *pseudoword* condition) based on concrete German nouns or well matched pseudowords. (**d) Perspective taking task.** In each trial, character A places a target object in a container. Thereafter, Character B changes the location of the target object. Character A has left the room (*false belief* condition) or watches the relocation of the object (*true belief* condition). Character A then searches for the target object at the location congruent with her / his knowledge (*expected*) or at the contradicting location (*unexpected*). Participants had to indicate via button press whether character A searched at the expected location or not. **Behavioral results** for each task are shown in the right panel, separately for each session. Single subject data is overlaid as circles.

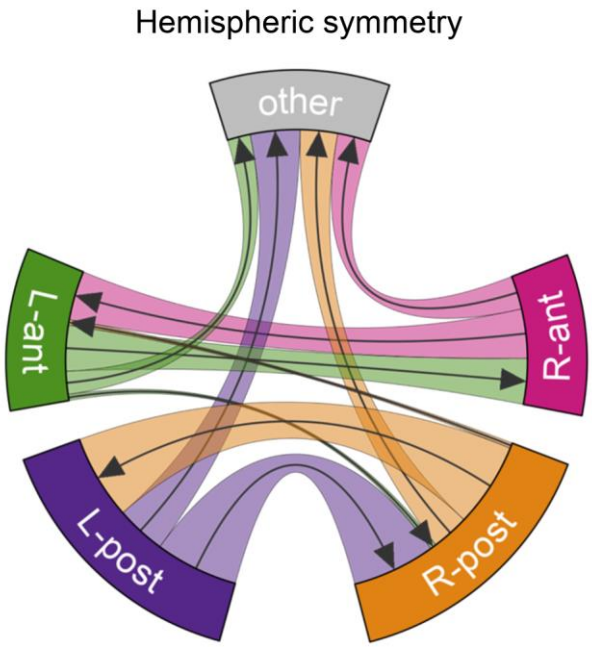

Figure 2–figure supplement 1. The final subregion solution shows a high degree of symmetry between hemispheres. Evidence supporting the hemispheric symmetry of the final two-subregion solution in the region of interest parcellation by clustering algorithms. Depicts which proportion of subregion-voxels falls into its homologue by flipping the x-axis, and which proportion falls into other areas.

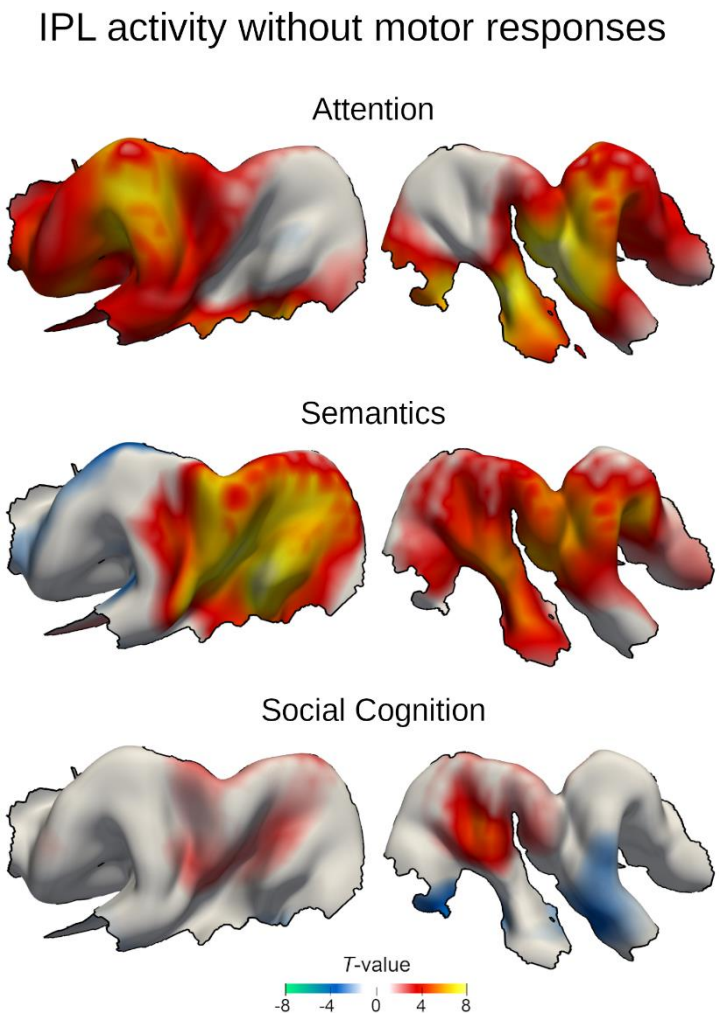

Figure 2–figure supplement 2. Task-evoked neural responses in the IPL region with explicit modelling of motor responses. Task-dependent BOLD responses from the model that explicitly accounts for general motor responses across tasks ($GLM_{cond+RT}$) resemble results from the original model (GLM_{cond}, Figure 1). Colors indicate unthresholded T-values. Warm colors: higher GLM beta estimates for the target conditions. Cold colors: higher GLM beta estimates for the control condition.

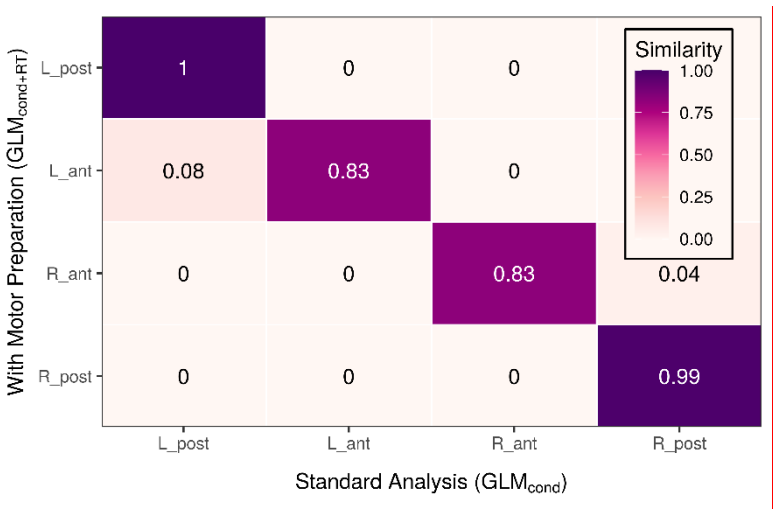

Figure 2–figure supplement 3. Explicitly modelling motor responses yields a similar clustering solution. Depicts the cluster-wise similarity of the parcellation solution based on the model that captured preparatory motor responses across tasks ($GLM_{cond+RT}$) compared to the basic model (GLM_{cond}).

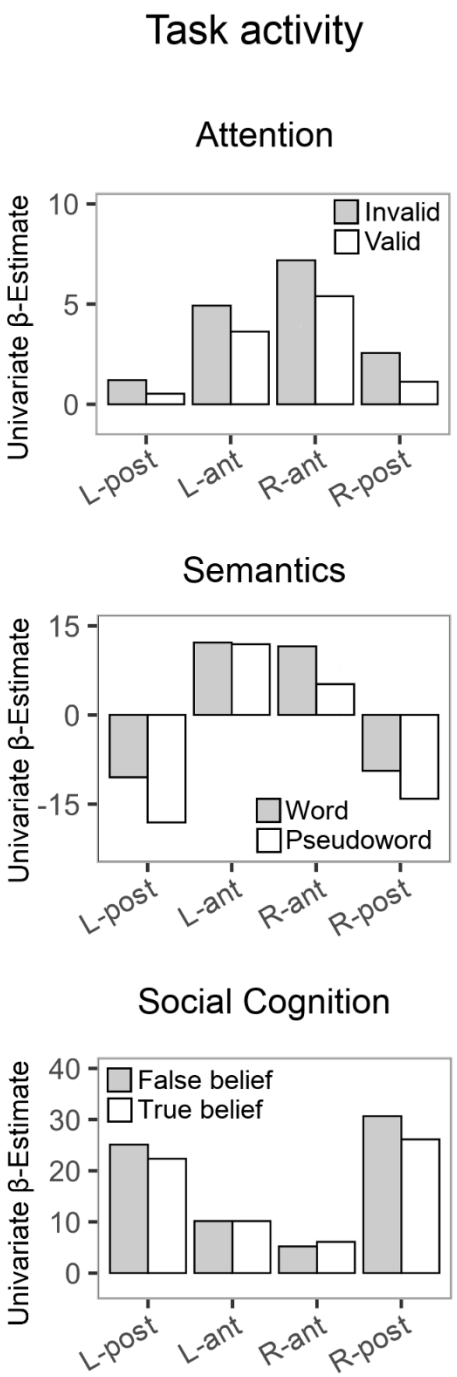

Figure 3–figure supplement 1. Neural activity estimates for the target and control conditions of the three tasks. For visualization purposes, beta estimates were extracted from GLM_{cond} at the center of mass for each IPL subregion.

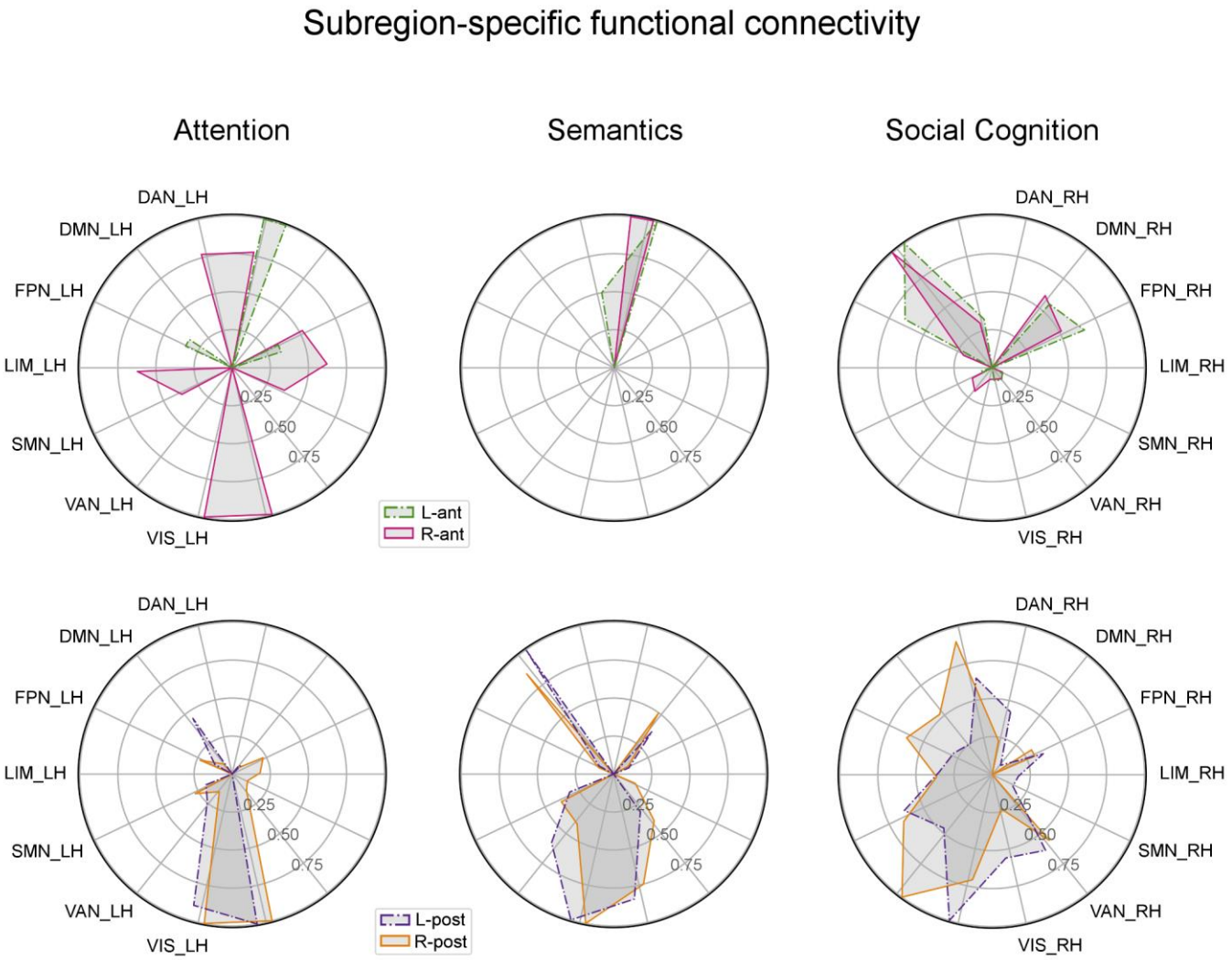

Figure 4–figure supplement 1. Functional connectivity between IPL subregions and large-scale brain networks. The preferred connectivity between IPL subregions and brain-wide cortical regions identified task-specific coupling motifs of the four subregions. Large-scale brain networks were split into their left and right hemispheric parts. Functional connectivity was normalized per subregion and task. Anterior IPL subregions (top row) connect in a hemisphere specific way, while posterior IPL subregions (bottom row) connect in a more bilateral-symmetric way. LH/RH: left/right hemispheric network parts. See main text for details on the connectivity metric. Networks acronyms as defined in the main text.

Table S1: Mass-univariate activations peaks for the three functional domains.

Region	Anatomical assignment	Hemis-phere	MNI coordinates X	Y	Z	T-value	Cluster size
Attentional reorienting							
Supramarginal gyrus	PFm	R	57	-48	24	9.68	181
Superior temporal gyrus / angular gyrus	PGa	R	63	-45	17	9.23	
Middle temporal gyrus / angular gyrus	PGp	R	48	-63	14	8.42	
Middle temporal gyrus		R	57	-57	-1	7.03	
Precuneus	7P	L	3	-54	52	9.46	123
Precuneus	5L	R	6	-60	59	8.27	
Precuneus	7A	L	12	-66	52	7.21	
Precentral gyrus		L	-27	-3	59	9.32	54
Superior frontal gyrus		R	30	-6	63	8.36	34
Middle frontal gyrus		R	36	-3	56	7.33	
Precentral gyrus		R	36	3	49	7.00	
Inferior parietal lobe	PF	L	-54	-42	38	7.35	33
Postcentral gyrus		L	-45	-33	49	7.04	
Inferior parietal lobule	hIP2	L	-45	-39	42	6.99	
Superior parietal lobe	hIP1	R	30	-48	42	10.10	31
Lexical decisions							
Angular gyrus	PGp	L	-51	-72	28	8.00	73
Angular gyrus	PGp	L	-39	-75	42	7.36	
Angular gyrus	PGa	L	-45	-57	35	7.22	
Middle cingulate gyrus	5M	L	-6	-30	42	9.07	50
Superior frontal gyrus		L	-18	36	49	7.94	34
Middle frontal gyrus		L	-27	24	52	6.64	
Perspective taking							
Supplementary motor cortex		L	-3	15	52	5.15	184
Superior medial gyrus		L	-6	24	42	4.37	
Superior frontal gyrus		L	-15	12	63	3.84	
Posterior medial frontal g.		R	12	6	52	3.73	
Inferior frontal gyrus	BA45	L	-45	24	31	5.11	59
Precentral gyrus		L	-39	3	42	4.77	45
not assigned		L	-45	6	56	3.84	
Precentral gyrus	BA44	L	-48	9	35	3.81	
Middle frontal gyrus		L	-42	3	52	3.72	
Angular gyrus	PGa	R	51	-60	31	5.15	32
Precuneus		R				4.50	31
Precuneus		L				3.98	
Middle temporal gyrus		R	54	-18	-15	4.68	20
Middle temporal gyrus		R	60	-15	-11	4.29	

Note: Attention and semantic tasks: thresholded at p=0.05, FWE corrected, cluster extent ≥20 voxels. Social cognition task: thresholded at p=0.001, uncorrected, cluster extent ≥20 voxels. Anatomical assignment according to SPM Anatomy toolbox (v. 22c).

Table S2: Intrinsic effective connectivity and task-specific self-connectivity modulation

Source subregion		Target subregion	Strength	95%-CI
Intrinsic connectivity				
L-ant	→	L-ant	-1.20	[-1.21; -1.20]
L-ant	→	L-post	-0.37	[-0.38; -0.37]
L-ant	→	R-ant	-0.33	[-0.33; -0.33]
L-ant	→	R-post	-0.56	[-0.56; -0.56]
L-post	→	L-ant	-0.05	[-0.06; -0.05]
L-post	→	L-post	-0.79	[-0.81; -0.79]
L-post	→	R-ant	0.15	[0.15; 0.16]
L-post	→	R-post	-0.29	[-0.29; -0.29]
R-ant	→	L-ant	-0.27	[-0.27; -0.27]
R-ant	→	L-post	0.38	[0.39; 0.39]
R-ant	→	R-ant	-1.13	[-1.14; -1.13]
R-ant	→	R-post	0.87	[0.87; 0.88]
R-post	→	L-ant	0.34	[0.34; 0.35]
R-post	→	L-post	0.42	[0.42; 0.43]
R-post	→	R-ant	-0.30	[-0.30; -0.30]
R-post	→	R-post	-1.14	[-1.15; -1.14]

Source subregion		Target subregion	Modulation strength	p-value
Self connectivity				
Semantics				
L-ant	→	L-ant	-5.53	0.0006
L-post	→	L-post	-6.88	0.0010
Social Cognition				
R-ant	→	R-ant	-4.01	0.0055

Note: Intrinsic connectivity parameters ('A-matrix') and significant modulatory parameters ('B-matrix', $\alpha \leq 0.01$) of self-connections. Strength is given as posterior expectation from the optimum Bayesian parameter average model. The 95% confidence intervals were built from the corresponding Bayesian parameter covariances and exceed zero for all parameters. P-values for self-connectivity are based on a random effects permutation test for the null hypothesis 'no parameter difference between tasks'.

References

Abdulrahman, H., & Henson, R. N. (2016). Effect of trial-to-trial variability on optimal event-related fMRI design: Implications for Beta-series correlation and multi-voxel pattern analysis. *NeuroImage*, *125*, 756–766. https://doi.org/10.1016/j.neuroimage.2015.11.009

Abraham, A., Pedregosa, F., Eickenberg, M., Gervais, P., Mueller, A., Kossaifi, J., Gramfort, A., Thirion, B., & Varoquaux, G. (2014). Machine learning for neuroimaging with scikit-learn. *Frontiers in Neuroinformatics*, *8*, 14. https://doi.org/10.3389/fninf.2014.00014

Ahrens, J., Geveci, B., & Law, C. (2005). ParaView: an end-user tool for large-data visualization. In Hansen, C.D. & Johnson, C.R. (Ed.), *The Visualization Handbook* (pp. 717–731). https://doi.org/10.1016/b978-012387582-2/50038-1

Amunts, K., & Zilles, K. (2001). Advances in cytoarchitectonic mapping of the human cerebral cortex. *Neuroimaging Clinics of North America*, *11*(2), 151–169, vii. https://www.ncbi.nlm.nih.gov/pubmed/11489732

Andersson, J. L. R., Skare, S., & Ashburner, J. (2003). How to correct susceptibility distortions in spin-echo echo-planar images: application to diffusion tensor imaging. *NeuroImage*, *20*(2), 870–888. https://doi.org/10.1016/S1053-8119(03)00336-7

Avants, B. B., Epstein, C. L., Grossman, M., & Gee, J. C. (2008). Symmetric diffeomorphic image registration with cross-correlation: evaluating automated labeling of elderly and neurodegenerative brain. *Medical Image Analysis*, *12*(1), 26–41. https://doi.org/10.1016/j.media.2007.06.004

Behzadi, Y., Restom, K., Liau, J., & Liu, T. T. (2007). A component based noise correction method (CompCor) for BOLD and perfusion based fMRI. *NeuroImage*, *37*(1), 90–101. https://doi.org/10.1016/j.neuroimage.2007.04.042

Binder, J. R., & Desai, R. H. (2011). The neurobiology of semantic memory. *Trends Cog. Sci.*, *15*(11), 527–536. https://doi.org/10.1016/j.tics.2011.10.001

Binder, J. R., Desai, R. H., Graves, W. W., & Conant, L. L. (2009). Where Is the semantic system?

A critical review and meta-analysis of 120 functional neuroimaging studies. *Cereb. Cortex*, *19*(12), 2767–2796. https://doi.org/10.1093/cercor/bhp055

Binder, J. R., McKiernan, K. A., Parsons, M. E., Westbury, C. F., Possing, E. T., Kaufman, J. N., & Buchanan, L. (2003). Neural correlates of lexical access during visual word recognition. *Journal of Cognitive Neuroscience*, *15*(3), 372–393. https://doi.org/10.1162/089892903321593108

Braga, R. M., DiNicola, L. M., & Buckner, R. L. (2019). Situating the left-lateralized language network in the broader organization of multiple specialized large-scale distributed networks. In *bioRxiv*. https://doi.org/10.1101/2019.12.11.873174

Brysbaert, M., Buchmeier, M., Conrad, M., Jacobs, A. M., Bölte, J., & Böhl, A. (2011). The word frequency effect: a review of recent developments and implications for the choice of frequency estimates in German. *Experimental Psychology*, *58*(5), 412–424. https://doi.org/10.1027/1618-3169/a000123

Buckner, R. L., & DiNicola, L. M. (2019). The brain's default network: updated anatomy, physiology and evolving insights. *Nat. Rev. Neurosci.*, *20*(10), 593–608. https://doi.org/10.1038/s41583-019-0212-7

Bzdok, D., Hartwigsen, G., Reid, A., Laird, A. R., Fox, P. T., & Eickhoff, S. B. (2016). Left inferior parietal lobe engagement in social cognition and language. *Neuroscience and Biobehavioral Reviews*, *68*, 319–334. https://doi.org/10.1016/j.neubiorev.2016.02.024

Bzdok, D., Langner, R., Schilbach, L., Jakobs, O., Roski, C., Caspers, S., Laird, A. R., Fox, P. T., Zilles, K., & Eickhoff, S. B. (2013). Characterization of the temporo-parietal junction by combining data-driven parcellation, complementary connectivity analyses, and functional decoding. *NeuroImage*, *81*, 381–392. https://doi.org/10.1016/j.neuroimage.2013.05.046

Bzdok, D., & Yeo, B. T. T. (2017). Inference in the age of big data: Future perspectives on neuroscience. *NeuroImage*, *155*, 549–564. https://doi.org/10.1016/j.neuroimage.2017.04.061

Caspers, S., Eickhoff, S. B., Geyer, S., Scheperjans, F., Mohlberg, H., Zilles, K., & Amunts, K.

(2008). The human inferior parietal lobule in stereotaxic space. *Brain Structure & Function*, *212*(6), 481–495. https://doi.org/10.1007/s00429-008-0195-z

Caspers, S., Eickhoff, S. B., Rick, T., von Kapri, A., Kuhlen, T., Huang, R., Shah, N. J., & Zilles, K. (2011). Probabilistic fibre tract analysis of cytoarchitectonically defined human inferior parietal lobule areas reveals similarities to macaques. *NeuroImage*, *58*(2), 362–380. https://doi.org/10.1016/j.neuroimage.2011.06.027

Chafee, M. V., Averbeck, B. B., & Crowe, D. A. (2007). Representing spatial relationships in posterior parietal cortex: single neurons code object-referenced position. *Cerebral Cortex* , *17*(12), 2914–2932. https://doi.org/10.1093/cercor/bhm017

Charrad, M., Ghazzali, N., Boiteau, V., & Niknafs, A. (2014). NbClust: An R package for determining the relevant number of clusters in a data set. *J. Stat. Softw.*, *61*(6), 1–36. https://doi.org/10.18637/jss.v061.i06

Corbetta, M., Patel, G., & Shulman, G. L. (2008). The reorienting system of the human brain: from environment to theory of mind. *Neuron*, *58*(3), 306–324. https://doi.org/10.1016/j.neuron.2008.04.017

Corbetta, M., Ramsey, L., Callejas, A., Baldassarre, A., Hacker, C. D., Siegel, J. S., Astafiev, S. V., Rengachary, J., Zinn, K., Lang, C. E., Connor, L. T., Fucetola, R., Strube, M., Carter, A. R., & Shulman, G. L. (2015). Common behavioral clusters and subcortical anatomy in stroke. *Neuron*, *85*(5), 927–941. https://doi.org/10.1016/j.neuron.2015.02.027

Corbin, N., Todd, N., Friston, K. J., & Callaghan, M. F. (2018). Accurate modeling of temporal correlations in rapidly sampled fMRI time series. *Human Brain Mapping*, *39*(10), 3884–3897. https://doi.org/10.1002/hbm.24218

Cox, R. W. (1996). AFNI: software for analysis and visualization of functional magnetic resonance neuroimages. *Computers and Biomedical Research, an International Journal*, *29*(3), 162–173. https://doi.org/10.1006/cbmr.1996.0014

Crowe, D. A., Averbeck, B. B., & Chafee, M. V. (2008). Neural ensemble decoding reveals a

correlate of viewer- to object-centered spatial transformation in monkey parietal cortex. *The Journal of Neuroscience: The Official Journal of the Society for Neuroscience*, *28*(20), 5218–5228. https://doi.org/10.1523/JNEUROSCI.5105-07.2008

Crowe, D. A., Averbeck, B. B., Chafee, M. V., & Georgopoulos, A. P. (2005). Dynamics of parietal neural activity during spatial cognitive processing. *Neuron*, *47*(6), 885–891. https://doi.org/10.1016/j.neuron.2005.08.005

Crowe, D. A., Chafee, M. V., Averbeck, B. B., & Georgopoulos, A. P. (2004). Neural activity in primate parietal area 7a related to spatial analysis of visual mazes. *Cerebral Cortex* , *14*(1), 23–34. https://doi.org/10.1093/cercor/bhg088

Dale, A. M., Fischl, B., & Sereno, M. I. (1999). Cortical surface-based analysis. I. Segmentation and surface reconstruction. *NeuroImage*, *9*(2), 179–194. https://doi.org/10.1006/nimg.1998.0395

Dronkers, N. F., Wilkins, D. P., Van Valin, R. D., Jr, Redfern, B. B., & Jaeger, J. J. (2004). Lesion analysis of the brain areas involved in language comprehension. *Cognition*, *92*(1-2), 145–177. https://doi.org/10.1016/j.cognition.2003.11.002

Durnez, J., Blair, R., & Poldrack, R. A. (2018). Neurodesign: optimal experimental designs for task fMRI. In *bioRxiv*. https://doi.org/10.1101/119594

Eickhoff, S. B., Stephan, K. E., Mohlberg, H., Grefkes, C., Fink, G. R., Amunts, K., & Zilles, K. (2005). A new SPM toolbox for combining probabilistic cytoarchitectonic maps and functional imaging data. *NeuroImage*, *25*(4), 1325–1335. https://doi.org/10.1016/j.neuroimage.2004.12.034

Esteban, O., Markiewicz, C. J., Blair, R. W., Moodie, C. A., Isik, A. I., Erramuzpe, A., Kent, J. D., Goncalves, M., DuPre, E., Snyder, M., Oya, H., Ghosh, S. S., Wright, J., Durnez, J., Poldrack, R. A., & Gorgolewski, K. J. (2019). fMRIPrep: a robust preprocessing pipeline for functional MRI. *Nature Methods*, *16*(1), 111–116. https://doi.org/10.1038/s41592-018-0235-4

Feinberg, D. A., Moeller, S., Smith, S. M., Auerbach, E., Ramanna, S., Gunther, M., Glasser, M. F.,

Miller, K. L., Ugurbil, K., & Yacoub, E. (2010). Multiplexed echo planar imaging for sub-second whole brain FMRI and fast diffusion imaging. *PloS One*, *5*(12), e15710. https://doi.org/10.1371/journal.pone.0015710

Fischl, B., Sereno, M. I., Tootell, R. B. H., & Dale, A. M. (1999). High-resolution intersubject averaging and a coordinate system for the cortical surface. *Hum. Brain Mapp.*, *8*(4), 272–284. https://doi.org/3.0.co;2-4">10.1002/(sici)1097-0193(1999)8:4<272::aid-hbm10>3.0.co;2-4

Fogassi, L., Ferrari, P. F., Gesierich, B., Rozzi, S., Chersi, F., & Rizzolatti, G. (2005). Parietal lobe: from action organization to intention understanding. *Science*, *308*(5722), 662–667. https://doi.org/10.1126/science.1106138

Fonov, V. S., Evans, A. C., McKinstry, R. C., Almli, C. R., & Collins, D. L. (2009). Unbiased nonlinear average age-appropriate brain templates from birth to adulthood. *Neuroimage*, *47*, S102. https://doi.org/10.1016/s1053-8119(09)70884-5

Fridriksson, J., Kjartansson, O., Morgan, P. S., Hjaltason, H., Magnusdottir, S., Bonilha, L., & Rorden, C. (2010). Impaired speech repetition and left parietal lobe damage. *The Journal of Neuroscience: The Official Journal of the Society for Neuroscience*, *30*(33), 11057–11061. https://doi.org/10.1523/JNEUROSCI.1120-10.2010

Fridriksson, J., Yourganov, G., Bonilha, L., Basilakos, A., Den Ouden, D.-B., & Rorden, C. (2016). Revealing the dual streams of speech processing. *Proceedings of the National Academy of Sciences of the United States of America*, *113*(52), 15108–15113. https://doi.org/10.1073/pnas.1614038114

Friederici, A. D. (2017). Evolution of the neural language network. *Psychon Bull. Rev.*, *24*(1), 41–47. https://doi.org/10.3758/s13423-016-1090-x

Friston, K., Moran, R., & Seth, A. K. (2013). Analysing connectivity with Granger causality and dynamic causal modelling. *Current Opinion in Neurobiology*, *23*(2), 172–178. https://doi.org/10.1016/j.conb.2012.11.010

Friston, K., & Penny, W. (2011). Post hoc Bayesian model selection. *NeuroImage*, *56*(4), 2089–

2099. https://doi.org/10.1016/j.neuroimage.2011.03.062

Fukuda, H., Ma, N., Suzuki, S., Harasawa, N., Ueno, K., Gardner, J. L., Ichinohe, N., Haruno, M., Cheng, K., & Nakahara, H. (2019). Computing social value conversion in the human brain. *The Journal of Neuroscience: The Official Journal of the Society for Neuroscience*, *39*(26), 5153–5172. https://doi.org/10.1523/JNEUROSCI.3117-18.2019

Gordon, E. M., Laumann, T. O., Marek, S., Raut, R. V., Gratton, C., Newbold, D. J., Greene, D. J., Coalson, R. S., Snyder, A. Z., Schlaggar, B. L., Petersen, S. E., Dosenbach, N. U. F., & Nelson, S. M. (2020). Default-mode network streams for coupling to language and control systems. *Proceedings of the National Academy of Sciences of the United States of America*. https://doi.org/10.1073/pnas.2005238117

Gorgolewski, K., Burns, C. D., Madison, C., Clark, D., Halchenko, Y. O., Waskom, M. L., & Ghosh, S. S. (2011). Nipype: a flexible, lightweight and extensible neuroimaging data processing framework in python. *Frontiers in Neuroinformatics*, *5*, 13. https://doi.org/10.3389/fninf.2011.00013

Greve, D. N., & Fischl, B. (2009). Accurate and robust brain image alignment using boundary-based registration. *NeuroImage*, *48*(1), 63–72. https://doi.org/10.1016/j.neuroimage.2009.06.060

Gu, Z., Gu, L., Eils, R., Schlesner, M., & Brors, B. (2014). circlize implements and enhances circular visualization in R. *Bioinformatics*, *30*(19), 2811–2812. https://doi.org/10.1093/bioinformatics/btu393

Hartigan, J. A., & Wong, M. A. (1979). Algorithm AS 136: A K-Means Clustering Algorithm. *J. Appl. Stat.*, *28*(1), 100. https://doi.org/10.2307/2346830

Hartwigsen, G. (2018). Flexible Redistribution in Cognitive Networks. *Trends Cogn. Sci.*, *22*(8), 687–698. https://doi.org/10.1016/j.tics.2018.05.008

Hartwigsen, G., Bzdok, D., Klein, M., Wawrzyniak, M., Stockert, A., Wrede, K., Classen, J., & Saur, D. (2017). Rapid short-term reorganization in the language network. *eLife*, *6*, 1–18.

https://doi.org/10.7554/eLife.25964

Hartwigsen, G., Stockert, A., Charpentier, L., Wawrzyniak, M., Klingbeil, J., Wrede, K., Obrig, H., & Saur, D. (2020). Short-term modulation of the lesioned language network. *eLife*, *9*. https://doi.org/10.7554/eLife.54277

Hartwigsen, G., Weigel, A., Schuschan, P., Siebner, H. R., Weise, D., Classen, J., & Saur, D. (2016). Dissociating parieto-frontal networks for phonological and semantic word decisions: A condition-and-perturb TMS study. *Cerebral Cortex* , *26*(6), 2590–2601. https://doi.org/10.1093/cercor/bhv092

Igelström, K. M., Webb, T. W., Kelly, Y. T., & Graziano, M. S. A. (2016). Topographical organization of attentional, social, and memory processes in the human temporoparietal cortex. *eNeuro*, *3*(2), 1–12. https://doi.org/10.1523/ENEURO.0060-16.2016

Jenkinson, M., Bannister, P., Brady, M., & Smith, S. (2002). Improved optimization for the robust and accurate linear registration and motion correction of brain images. *NeuroImage*, *17*(2), 825–841. https://doi.org/10.1016/s1053-8119(02)91132-8

Kanske, P., & Kotz, S. A. (2011). Cross-modal validation of the Leipzig Affective Norms for German (LANG). *Behavior Research Methods*, *43*(2), 409–413. https://doi.org/10.3758/s13428-010-0048-6

Kernbach, J. M., Yeo, B. T. T., Smallwood, J., Margulies, D. S., Thiebaut de Schotten, M., Walter, H., Sabuncu, M. R., Holmes, A. J., Gramfort, A., Varoquaux, G., Thirion, B., & Bzdok, D. (2018). Subspecialization within default mode nodes characterized in 10,000 UK Biobank participants. *Proceedings of the National Academy of Sciences of the United States of America*, *115*(48), 12295–12300. https://doi.org/10.1073/pnas.1804876115

Keuleers, E., & Brysbaert, M. (2010). Wuggy: a multilingual pseudoword generator. *Behavior Research Methods*, *42*(3), 627–633. https://doi.org/10.3758/BRM.42.3.627

Klein, A., Ghosh, S. S., Bao, F. S., Giard, J., Häme, Y., Stavsky, E., Lee, N., Rossa, B., Reuter, M., Chaibub Neto, E., & Keshavan, A. (2017). Mindboggling morphometry of human brains. *PLoS*

Computational Biology, *13*(2), e1005350. https://doi.org/10.1371/journal.pcbi.1005350

Krall, S. C., Volz, L. J., Oberwelland, E., Grefkes, C., Fink, G. R., & Konrad, K. (2016). The right temporoparietal junction in attention and social interaction: a transcranial magnetic stimulation study. *Human Brain Mapping*, *37*(2), 796–807. https://doi.org/10.1002/hbm.23068

Kravitz, D. J., Saleem, K. S., Baker, C. I., & Mishkin, M. (2011). A new neural framework for visuospatial processing. *Nature Reviews. Neuroscience*, *12*(4), 217–230. https://doi.org/10.1038/nrn3008

Lambon Ralph, M. A., & Patterson, K. (2008). Generalization and differentiation in semantic memory: insights from semantic dementia. *Annals of the New York Academy of Sciences*, *1124*, 61–76. https://doi.org/10.1196/annals.1440.006

Marcus, D. S., Wang, T. H., Parker, J., Csernansky, J. G., Morris, J. C., & Buckner, R. L. (2007). Open Access Series of Imaging Studies (OASIS): cross-sectional MRI data in young, middle aged, nondemented, and demented older adults. *Journal of Cognitive Neuroscience*, *19*(9), 1498–1507. https://doi.org/10.1162/jocn.2007.19.9.1498

Margulies, D. S., Ghosh, S. S., Goulas, A., Falkiewicz, M., Huntenburg, J. M., Langs, G., Bezgin, G., Eickhoff, S. B., Castellanos, F. X., Petrides, M., Jefferies, E., & Smallwood, J. (2016). Situating the default-mode network along a principal gradient of macroscale cortical organization. *Proceedings of the National Academy of Sciences of the United States of America*, *113*(44), 12574–12579. https://doi.org/10.1073/pnas.1608282113

Mars, R. B., Jbabdi, S., Sallet, J., O'Reilly, J. X., Croxson, P. L., Olivier, E., Noonan, M. P., Bergmann, C., Mitchell, A. S., Baxter, M. G., Behrens, T. E. J., Johansen-Berg, H., Tomassini, V., Miller, K. L., & Rushworth, M. F. S. (2011). Diffusion-weighted imaging tractography-based parcellation of the human parietal cortex and comparison with human and macaque resting-state functional connectivity. *J. Neurosci.*, *31*(11), 4087–4100. https://doi.org/10.1523/jneurosci.5102-10.2011

Mars, R. B., Sallet, J., Neubert, F.-X., & Rushworth, M. F. S. (2013). Connectivity profiles reveal

the relationship between brain areas for social cognition in human and monkey temporoparietal cortex. *Proceedings of the National Academy of Sciences of the United States of America*, *110*(26), 10806–10811. https://doi.org/10.1073/pnas.1302956110

Mazziotta, J., Toga, A., Evans, A., Fox, P., Lancaster, J., Zilles, K., Woods, R., Paus, T., Simpson, G., Pike, B., Holmes, C., Collins, L., Thompson, P., MacDonald, D., Iacoboni, M., Schormann, T., Amunts, K., Palomero-Gallagher, N., Geyer, S., … Mazoyer, B. (2001). A probabilistic atlas and reference system for the human brain: International Consortium for Brain Mapping (ICBM). *Philosophical Transactions of the Royal Society of London. Series B, Biological Sciences*, *356*(1412), 1293–1322. https://doi.org/10.1098/rstb.2001.0915

Mirman, D., & Graziano, K. M. (2012). Damage to temporo-parietal cortex decreases incidental activation of thematic relations during spoken word comprehension. *Neuropsychologia*, *50*(8), 1990–1997. https://doi.org/10.1016/j.neuropsychologia.2012.04.024

Morrow, L. A., & Ratcliff, G. (1998). The disengagement of covert attention and the neglect syndrome. *Psychobiology* , *16*(3), 261–269.

Oldfield, R. C. (1971). The assessment and analysis of handedness: the Edinburgh inventory. *Neuropsychologia*, *9*(1), 97–113. https://doi.org/10.1016/0028-3932(71)90067-4

Oligschläger, S., Xu, T., Baczkowski, B. M., Falkiewicz, M., Falchier, A., Linn, G., & Margulies, D. S. (2018). Gradients of connectivity distance in the cerebral cortex of the macaque monkey. *Brain Structure & Function*, *224*, 925–935. https://doi.org/10.1101/467860

Orban, G. A., Van Essen, D., & Vanduffel, W. (2004). Comparative mapping of higher visual areas in monkeys and humans. *Trends in Cognitive Sciences*, *8*(7), 315–324. https://doi.org/10.1016/j.tics.2004.05.009

Pedregosa, F., Varoquaux, G., Gramfort, A., Michel, V., Thirion, B., Grisel, O., Blondel, M., Prettenhofer, P., Weiss, R., Dubourg, V., Vanderplas, J., Passos, A., Cournapeau, D., Brucher, M., Perrot, M., & Duchesnay, E. (2011). Scikit-learn: machine Learning in Python. *Journal of Machine Learning Research: JMLR*, *12*, 2825–2830.

Power, J. D., Barnes, K. A., Snyder, A. Z., Schlaggar, B. L., & Petersen, S. E. (2012). Spurious but systematic correlations in functional connectivity MRI networks arise from subject motion. *NeuroImage*, *59*(3), 2142–2154. https://doi.org/10.1016/j.neuroimage.2011.10.018

Power, J. D., Mitra, A., Laumann, T. O., Snyder, A. Z., Schlaggar, B. L., & Petersen, S. E. (2014). Methods to detect, characterize, and remove motion artifact in resting state fMRI. *NeuroImage*, *84*, 320–341. https://doi.org/10.1016/j.neuroimage.2013.08.048

Rosa, M. J., Friston, K., & Penny, W. (2012). Post-hoc selection of dynamic causal models. *Journal of Neuroscience Methods*, *208*(1), 66–78. https://doi.org/10.1016/j.jneumeth.2012.04.013

Rothmayr, C., Sodian, B., Hajak, G., Döhnel, K., Meinhardt, J., & Sommer, M. (2011). Common and distinct neural networks for false-belief reasoning and inhibitory control. *NeuroImage*, *56*(3), 1705–1713. https://doi.org/10.1016/j.neuroimage.2010.12.052

Rozzi, S., Ferrari, P. F., Bonini, L., Rizzolatti, G., & Fogassi, L. (2008). Functional organization of inferior parietal lobule convexity in the macaque monkey: electrophysiological characterization of motor, sensory and mirror responses and their correlation with cytoarchitectonic areas. *The European Journal of Neuroscience*, *28*(8), 1569–1588. https://doi.org/10.1111/j.1460-9568.2008.06395.x

Rushworth, M. F., Ellison, A., & Walsh, V. (2001). Complementary localization and lateralization of orienting and motor attention. *Nature Neuroscience*, *4*(6), 656–661. https://doi.org/10.1038/88492

Samson, D., Apperly, I. A., Chiavarino, C., & Humphreys, G. W. (2004). Left temporoparietal junction is necessary for representing someone else's belief. *Nat. Neurosci.*, *7*(5), 499–500. https://doi.org/10.1038/nn1223

Schaefer, A., Kong, R., Gordon, E. M., Laumann, T. O., Zuo, X.-N., Holmes, A. J., Eickhoff, S. B., & Yeo, B. T. T. (2018). Local-global parcellation of the human cerebral cortex from intrinsic functional connectivity MRI. *Cerebral Cortex* , *28*(9), 3095–3114. https://doi.org/10.1093/cercor/bhx179

Schuwerk, T., Schurz, M., Müller, F., Rupprecht, R., & Sommer, M. (2017). The rTPJ's overarching cognitive function in networks for attention and theory of mind. *Soc. Cogn. Affect. Neurosci.*, *12*(1), 157–168. https://doi.org/10.1093/scan/nsw163

Schwartz, M. F., Kimberg, D. Y., Walker, G. M., Brecher, A., Faseyitan, O. K., Dell, G. S., Mirman, D., & Coslett, H. B. (2011). Neuroanatomical dissociation for taxonomic and thematic knowledge in the human brain. *Proceedings of the National Academy of Sciences of the United States of America*, *108*(20), 8520–8524. https://doi.org/10.1073/pnas.1014935108

Seghier, M. L. (2013). The angular gyrus: multiple functions and multiple subdivisions. *The Neuroscientist: A Review Journal Bringing Neurobiology, Neurology and Psychiatry*, *19*(1), 43–61. https://doi.org/10.1177/1073858412440596

Seghier, M. L., & Friston, K. J. (2013). Network discovery with large DCMs. *NeuroImage*, *68*, 181–191. https://doi.org/10.1016/j.neuroimage.2012.12.005

Sliwinska, M. W., James, A., & Devlin, J. T. (2015). Inferior parietal lobule contributions to visual word recognition. *Journal of Cognitive Neuroscience*, *27*(3), 593–604. https://doi.org/10.1162/jocn_a_00721

Snyder, L. H., Grieve, K. L., Brotchie, P., & Andersen, R. A. (1998). Separate body- and world-referenced representations of visual space in parietal cortex. *Nature*, *394*(6696), 887–891. https://doi.org/10.1038/29777

Sommer, M., Meinhardt, J., Eichenmüller, K., Sodian, B., Döhnel, K., & Hajak, G. (2010). Modulation of the cortical false belief network during development. *Brain Research*, *1354*, 123–131. https://doi.org/10.1016/j.brainres.2010.07.057

Thiebaut de Schotten, M., Tomaiuolo, F., Aiello, M., Merola, S., Silvetti, M., Lecce, F., Bartolomeo, P., & Doricchi, F. (2014). Damage to white matter pathways in subacute and chronic spatial neglect: a group study and 2 single-case studies with complete virtual "in vivo" tractography dissection. *Cerebral Cortex* , *24*(3), 691–706. https://doi.org/10.1093/cercor/bhs351

Thirion, B., Varoquaux, G., Dohmatob, E., & Poline, J.-B. (2014). Which fMRI clustering gives good brain parcellations? *Frontiers in Neuroscience*, *8*, 167. https://doi.org/10.3389/fnins.2014.00167

Toga, A. W., & Thompson, P. M. (2003). Mapping brain asymmetry. *Nature Reviews. Neuroscience*, *4*(1), 37–48. https://doi.org/10.1038/nrn1009

Tustison, N. J., Avants, B. B., Cook, P. A., Zheng, Y., Egan, A., Yushkevich, P. A., & Gee, J. C. (2010). N4ITK: improved N3 bias correction. *IEEE Transactions on Medical Imaging*, *29*(6), 1310–1320. https://doi.org/10.1109/TMI.2010.2046908

Van Essen, D. C., & Dierker, D. L. (2007). Surface-based and probabilistic atlases of primate cerebral cortex. *Neuron*, *56*(2), 209–225. https://doi.org/10.1016/j.neuron.2007.10.015

Vázquez-Rodríguez, B., Suárez, L. E., Markello, R. D., Shafiei, G., Paquola, C., Hagmann, P., van den Heuvel, M. P., Bernhardt, B. C., Nathan Spreng, R., & Misic, B. (2019). Gradients of structure–function tethering across neocortex. *Proceedings of the National Academy of Sciences of the United States of America*, *116*(42), 21219–21227. https://doi.org/10.1073/pnas.1903403116

Wu, J., Ngo, G. H., Greve, D., Li, J., He, T., Fischl, B., Eickhoff, S. B., & Yeo, B. T. T. (2018). Accurate nonlinear mapping between MNI volumetric and FreeSurfer surface coordinate systems. *Human Brain Mapping*, *39*(9), 3793–3808. https://doi.org/10.1002/hbm.24213

Xia, M., Wang, J., & He, Y. (2013). BrainNet Viewer: a network visualization tool for human brain connectomics. *PloS One*, *8*(7), e68910. https://doi.org/10.1371/journal.pone.0068910

Xu, T., Nenning, K.-H., Schwartz, E., Hong, S.-J., Vogelstein, J. T., Goulas, A., Fair, D. A., Schroeder, C. E., Margulies, D. S., Smallwood, J., Milham, M. P., & Langs, G. (2020). Cross-species functional alignment reveals evolutionary hierarchy within the connectome. *NeuroImage*, *223*, 117346. https://doi.org/10.1016/j.neuroimage.2020.117346

Yeo, B. T. T., Krienen, F. M., Sepulcre, J., Sabuncu, M. R., Lashkari, D., Hollinshead, M., Roffman, J. L., Smoller, J. W., Zöllei, L., Polimeni, J. R., Fischl, B., Liu, H., & Buckner, R. L.

(2011). The organization of the human cerebral cortex estimated by intrinsic functional connectivity. *Journal of Neurophysiology*, *106*(3), 1125–1165. https://doi.org/10.1152/jn.00338.2011

Zeidman, P., Jafarian, A., Corbin, N., Seghier, M. L., Razi, A., Price, C. J., & Friston, K. J. (2019). A guide to group effective connectivity analysis, part 1: First level analysis with DCM for fMRI. *Neuroimage*, *200*, 174–190. https://doi.org/10.1016/j.neuroimage.2019.06.031

Zhang, Y., Brady, M., & Smith, S. (2001). Segmentation of brain MR images through a hidden Markov random field model and the expectation-maximization algorithm. *IEEE Transactions on Medical Imaging*, *20*(1), 45–57. https://doi.org/10.1109/42.906424

Zilles, K., & Amunts, K. (2010). Centenary of Brodmann's map — conception and fate. *Nat. Rev. Neurosci.*, *11*(2), 139–145. https://doi.org/10.1038/nrn2776